AD-A066 721 CALSPAN ADVANCED TECHNOLOGY CENTER BUFFALO NY F/6 20/5
MEASUREMENT OF KINETIC RATES FOR CARBON MONOXIDE LASER SYSTEMS.(U)
NOV 78 J W RICH, R C BERGMAN, M J WILLIAMS F49620-77-C-0020
UNCLASSIFIED CALSPAN-WG-6021-A-2 AFOSR-TR-79-0283 NL

| OF |
ADA
066721

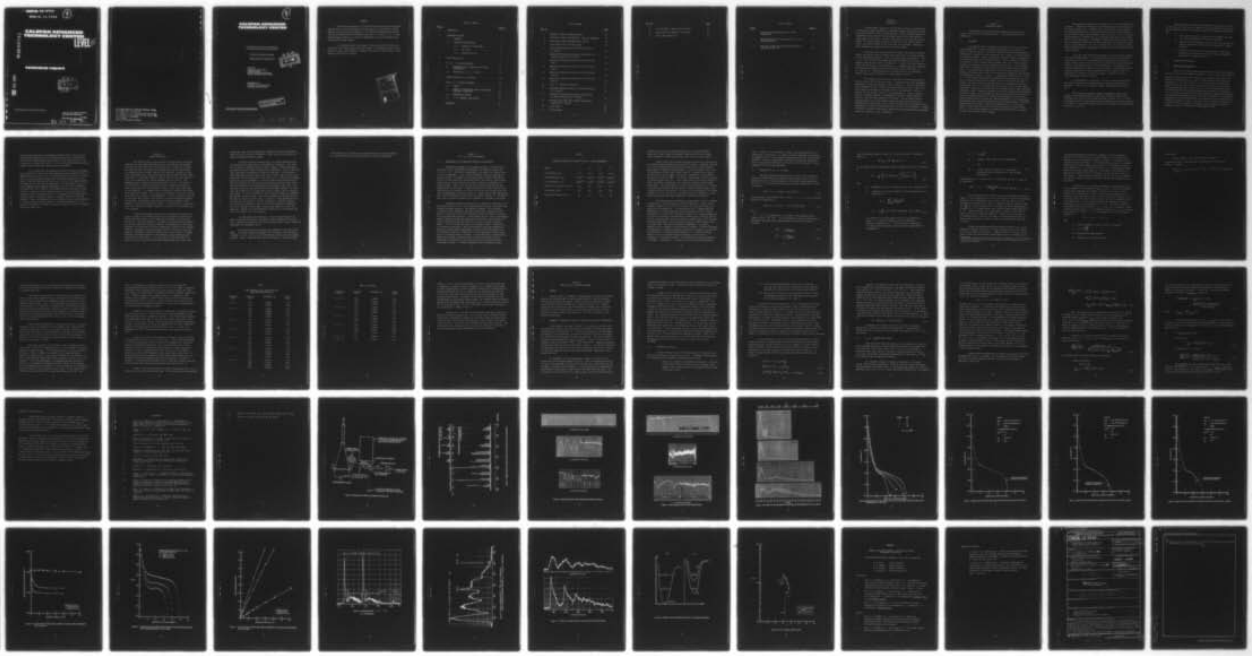

END
DATE
FILMED
5-79
DDC

CALSPAN ADVANCED TECHNOLOGY CENTER

LEVEL II

technical report

A DIVISION OF CALSPAN CORPORATION
AN ARVIN COMPANY P.O. BOX 400 BUFFALO, NEW YORK 14225

AIR FORCE OFFICE OF SCIENTIFIC RESEARCH (AFSC)
NOTICE OF TRANSMITTAL TO DDC
This technical report has been reviewed and is approved for public release IAW AFR 190-12 (7b).
Distribution is unlimited.
A. D. BLOSE
Technical Information Officer

(4)

CALSPAN ADVANCED TECHNOLOGY CENTER

MEASUREMENT OF KINETIC RATES FOR CARBON MONOXIDE LASER SYSTEMS

J.W. Rich, R.C. Bergman, M.J. Williams

Calspan Report No. WG-6021-A-2

Prepared for:

UNITED STATES AIR FORCE
PHYSICS DIVISION
OFFICE OF SCIENTIFIC RESEARCH
BOLLING AIR FORCE BASE, DC 20332

NOVEMBER 1978
CONTRACT NO. F49620-77-C-0020
INTERIM SCIENTIFIC REPORT

A DIVISION OF CALSPAN CORPORATION
AN ARVIN COMPANY P.O. BOX 400 BUFFALO, NEW YORK 14225

ABSTRACT

The vibration-translation (V-T) deactivation rates for high vibrational quantum levels of carbon monoxide have been measured for collisions of carbon monoxide with argon at room temperature. The rates are quantum-state-resolved and have now been measured for quantum levels from V = 10 up to V = 42. A laser optical pumping technique is used; the measurements are in an environment free of electric discharge effects.

In a related phase of the program, evidence of molecular vibration-to-electronic (V-E) energy transfer has been adduced. Preliminary analysis of this process is given, and potential V-E transfer laser action, based on highly vibrationally excited CO, is assessed.

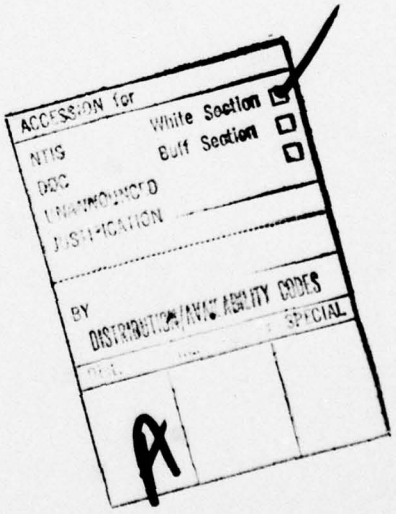

TABLE OF CONTENTS

LIST OF FIGURES

LIST OF TABLES

Section 1
INTRODUCTION

The experiments reported in the following sections are measurements of the rate of energy transfer from high-quantum-number vibrational levels of the ground electronic state of carbon monoxide. Energy transfer among the CO vibrational states, and from the vibrational states to the other molecular energy modes of translation, rotation, and electronic excitation has been observed. The present report is for the second year of this ongoing project; there is an interim report[1] for the first year of the program. Reference 1 gives background and original motivation for the program.

The first year's studies under this program concentrated on measurement of the specific rates of vibration-to-translation (V-T) energy transfer in CO-Ar and CO-He collisions, for CO vibrational energy levels from V = 20 to V = 40. This work has been extended and continued during the past year. In addition, the past year's work has emphasized 1) study of the early stages of vibrational excitation of the CO molecules; 2) computer modeling of vibrationally excited CO molecule kinetics using the newly derived rate data; and 3) study of V-E transfer processes, including analysis of potential V-E transfer lasers using vibrationally excited diatomic molecules.

The following sections of this report detail work performed during the past year in each of the above areas. A recapitulation of the experimental method used in these measurements is given in Section 2. Section 3 describes recent experimental work in improving the techniques used, and in study of the early stages of vibrational activation of CO in our experiment. Section 4 presents the new results in CO-Ar V-T rate measurements. Section 5 outlines results of computer modeling of vibrationally excited CO energy transfer kinetics, using the newly-acquired V-T rate data. The concluding Section 6 presents analysis of the V-E energy transfer processes observed during our experiments last year; there is also a detailed assessment of the potential for developing a V-E transfer laser operating at visible or UV wavelengths. A summary of research personnel, publications, patents and meeting presentations performed under this contract is given in Appendix A.

Section 2
EXPERIMENTAL METHOD

The descriptions of the experimental apparatus and technique contained in this section are repeated from Ref. 1, and are included here for completeness.

2.1 APPARATUS

The apparatus used in the present experiments is basically a flowing gas absorption cell, in which a nonequilibrium distribution of vibrational energy is created in CO gas. This type of nonequilibrium vibrational population distribution is created by vibration-vibration (V-V) inelastic collisions between the diatomic molecules, in which a quantum of vibrational energy is exchanged by the vibrational modes of the collision partners. Such an inelastic collision is not typically an exact resonance energy transfer event, due to energy mismatch caused by the anharmonicity of the vibrational quantum states. This resonance defect must be supplied by energy exchange with the translational and rotational modes. At low translational temperature, collisions between molecules in anharmonic vibrational states m and n ($m > n$) have greater probability for producing V-V transitions to states $m + 1$ and $n - 1$ compared with transitions to $m - 1$ and $n + 1$. This biasing occurs because the former transition results in a net surplus of vibrational energy which is readily fed into the translational mode. In contrast, the latter transition requires energy to be supplied from the translational mode, which, at low temperature, has relatively little available energy. Accordingly, a population inversion tends to be created among the upper anharmonic vibrational states. Theoretical treatment of the kinetic equations governing these processes by Treanor, Rich and Rehm[2] has shown that under the stated conditions of high vibrational energy and low translational temperature, the vibrational population distribution created by this exchange mechanism will be non-Boltzmann, and characterized by relative overpopulation of the higher anharmonic vibrational quantum states with respect to the lowest vibrational states. This kinetic effect has been found to be the major inversion mechanism in carbon monoxide lasers. In the present apparatus, the nonequilibrium distribution is produced in steady state by direct optical pumping.

The experimental apparatus, as presently set up, is shown schematically in Figure 1. Premixed carbon monoxide, helium and argon gases flow through the 25-cm-long absorption cell. Radiation from an electrically excited supersonic flow cw carbon monoxide laser is admitted along the axis of the cell through a calcium fluoride window; the beam diameter nearly fills the 0.95-cm cell diameter. The pump radiation is absorbed into the vibrational energy mode of the CO component of the cell gas mixture. The degree of absorption of the laser beam by the gases is determined by measuring the power incident upon and transmitted through the cell using thermopiles. The cell is equipped with calcium fluoride windows along its length to permit spectroscopic monitoring of the carbon monoxide vibrational excitation.

A 3/4 meter Spex scanning monochromator is used as the basic spectroscopic monitoring instrument. To record spontaneous infrared emission from the side windows of the cell, the monochromator is equipped with a 300 line/m.m. optical grating, blazed at 4 μm, and an InSb liquid-nitrogen-cooled photovoltaic detector. The radiative signal into the monochromator is interrupted with a synchronous-motor-driven chopper, driven at 800 hertz. Chopped output from the detector is amplified by a Princeton Applied Research Corporation Model 124 phase-sensitive amplifier; the amplified signal is recorded on a Varian Corporation Model 2400 chart recorder.

The monochromator is evacuated. The relative amplitude response of the system is determined in standard fashion by scanning a calibrated black body source. Details of the instrument response determination are given in Ref. 1.

With this optical pumping technique, measurements using the monochromator system described above have shown that vibrational energy of the carbon monoxide in the cell can be made quite high, typically 0.3 - 0.4 eV per CO molecule, while the translational-rotational temperature can be kept relatively low (0[300°K]). This nonequilibrium condition is maintained in the steady state in the cell by the flow.

There are several advantages of this method of vibrational excitation for the study of kinetic rates, in contrast to the usual methods involving direct electric-discharge excitation or thermal excitation. The principle advantages are:

(1) Vibrational excitation is achieved in an environment free from the kinetic complications of ionized gas processes.

(2) Higher levels of vibrational excitation can be achieved than are typically obtained in either electric discharge or by thermal excitation.

(3) Pressures and gas mixtures can be varied over a large range. Conditions can be achieved that would be totally incompatible with electric discharge stability.

2.2 OPERATING CHARACTERISTICS

2.2.1 Conditions of Measurement

Table 1 lists typical operating parameters of the pump laser and absorption cell for the rate measurements reported here. The c.w. pump laser output is broad-band, distributed over more than thirty CO vibrational-rotational lines ranging in wavelength from 4.8 to 5.5 μm. These lines are from vibrational transitions v=3 $\longrightarrow$ 2 up to v=15 $\longrightarrow$ 14. With the addition of argon in the amount listed in the table, the heat capacity of the gas flow is quite high; the maximum temperature rise that could occur if all the absorbed laser power were relaxed into the translational and rotational gas modes at equilibrium is 71°K. In practice, the actual translational-rotational temperature rise throughout the region of measurement in the cell is far less than this. Spectroscopic measurement of the relative rotational line intensity of CO and other molecular emitters (see Section 3.2 below) in the flow allows a rotational temperature of $\sim$ 300°K $\pm$10°K to be inferred. Accordingly, the rate measurements given in subsequent sections are reported for a temperature of 300°K.

TABLE 1

TYPICAL OPERATING CONDITIONS FOR V-T
RATE MEASUREMENT EXPERIMENTS

Laser Power	205 Watts
Laser Power Absorbed	39 Watts
Cell Pressure	760 Torr
Cell Gas Inlet Temperature	300°K
Cell Flow Velocity	907 cm/sec
Cell Gas Concentrations:	
Carbon Monoxide	2.10×10^{17} cm^{-3}
Helium	1.30×10^{18} cm^{-3}
Argon	2.30×10^{19} cm^{-3}

2.2.2 Test Gases

The gases used in the cell were Air Products Co. UHP grade CO, nominal purity 99.8%; Linde Corporation H.P. grade Ar, nominal purity 99.996%; Linde Corporation H.P. grade He, nominal purity 99.995%. Before entering the cell, the CO and Ar gases pass through a system of double traps. The first traps consist of a 10' long helical coil of 3/8" tubing, filled with alumina pellets. These coils are wall-cooled by a dry ice/methanol bath. The second set of traps consist of 10' long coils filled with copper wool; these coils are wall-cooled by baths of freezing propanol slush. This system is a development of the method originally proposed by Millikan.[3] The system is designed to reduce the concentrations of condensable impurities, most especially water vapor and hydrocarbons other than CH_4, to less than 0.5 ppm. The details of the gas purification system used, and an assessment of the influence of residual impurities, have been given in Ref. 1.

2.2.3 Absorption Process

It can be seen from Table 1 that, for the conditions listed there, 19% of the pump laser power is absorbed. The details of the mechanism by which the pump laser beam is absorbed at the relatively low cell pressure and temperature of Table 1 remain to be clarified. As noted previously, the output from the pump laser beam is distributed among approximately 30 P-branch rotation-vibration lines from the $v=3 \rightarrow 2$ to the $v=15 \rightarrow 14$ vibrational transition, the most intense lines being on the lower vibrational transitions. After transmission through the CO in the cell, it is observed that the lowest level transitions, beginning with $v=3 \rightarrow 2$, are the most strongly absorbed. The extent of absorption decreases with increasing vibrational band quantum number, with transitions above v=11 being only slightly attenuated. The total amount of absorption increases with decreasing total gas pressure; while approximately 19% of the pump beam is absorbed at the one atmosphere conditions of Table 1, more than 70% of the pump beam is absorbed in 40 torr of pure CO, without any diluent. Figure 2 shows the spectral dependence of the absorption of the pump laser radiation for such a low pressure case. The output of the pump laser is displayed on the lower trace;

the upper trace shows what is transmitted through 40 torr of CO in the cell. The variation of absorption with vibrational quantum level is qualitatively similar to the higher pressure cases; however, at the lower pressure, it can be seen that all lines on the $v=3 \rightarrow 2$, $4 \rightarrow 3$, and $5 \rightarrow 4$ bands have been entirely absorbed, and the other lower bands are greatly attenuated.

It is evident that the absorbing transitions occurring in the pumped gas are identical to those of the laser emissions; given the nature of the V-V pumped distribution in the cell, it is predictable that the lower level transitions will be more readily absorbed, due to the higher populations of these states. Since the laser does not emit on the $v=1 \rightarrow 0$ or $v=2 \rightarrow 1$ bands, calculation shows the cell gas would be transparent to the pump radiation, level $v=2$ of the pumped gas being negligibly populated at the cell kinetic temperature of approximately 300°K. However, some triggering process does occur to populate the $v=2$ level in the small amount necessary to cause significant $v=2 \rightarrow 3$ absorption; after this triggering occurs, V-V pumping insures an exponentially increasing number of molecules capable of resonance absorption of the pump radiation. Thus a small number of initial absorbers, such as could be provided by localized heating or the absorption by the natural abundance (1%) of the more nearly resonant $C^{13}O$ isotope, will increase rapidly to provide the observed large total absorptions.

Section 3
LASER STABILIZATION

The supersonic flow CO laser used for an optical pump in the present experiments has good amplitude stability; short term stability (millisecond-time scale) is well within ±10%; long term stability is within ±3%. However, the laser does exhibit rotational line jumping; while the laser output power per vibrational band is roughly constant, the oscillation is usually on three or four rotational lines in each band, and peak power in each band varies among these lines. An individual rotational line may actually cease oscillation entirely, and an adjacent line, having comparable gain, may turn on. This phenomenon causes a long-term amplitude oscillation of ±1-3%. The period of this oscillation is rather long, being of several seconds duration when the laser is just turned on, and increasing to almost a minute after several minutes of operation. It is apparent that this behavior is caused by the cooling of the laser mirror mounts. The in-cavity gas temperature is near 45°K, and the mirror mounts are initially at room temperature. As they are cooled by the cold gas flow, they begin to move in one direction, causing the observed rotational line shifting. The movement is most rapid in the initial moments of laser operation, when thermal gradients are largest. As the laser cools, mirror movements slows, causing the observed increase in the period of the oscillation due to line jumping.

In previous experiments where the energy absorbed per CO molecule in the cell is high, the gas rapidly becomes fully vibrationally excited and the detected sidelight emission is not significantly perturbed by the pump laser oscillations. Thus, the inferred V-T and radiative rates based on this emission also are not significantly affected. However, in experiments where the energy absorbed is low and the gas is not fully vibrationally excited, the IR sidelight radiation is observed to oscillate in phase with the oscillations of the pump radiation. Furthermore, instead of exhibiting the ±3% oscillation of the pump radiation, the emitted radiation in this upstream, initial absorption region may oscillate by ±50% or more. It is clear that this amplifying effect is caused by the oscillations of the shortest-wavelength pump laser lines; these

are the only lines that are significantly absorbed in the initial absorption region of the cell, and any fluctuations in these lines can cause large variations in IR emission from this region.

In order to stabilize the pump laser, the totally reflecting mirror in the optical cavity was mounted on a piezoelectric translator. This translator is part of a feedback loop which senses a change in laser output power and adjusts the cavity length to maximize that laser power. Initially the total laser output power was monitored to adjust the translator. This resulted in fairly good stabilization as can be seen in Fig. 3 which shows the total laser output power (a), the output power of one laser line (b), and the cell sidelight emission at a given wavelength (c), initially without laser stabilization and then with stabilization. The arrows on the stabilized portions of the curves indicate the points at which the feedback loop performed a "mode jump". This mode jump occurs when the translator reaches its maximum extension. The translator then "jumps" back to a preset position which ideally results in maximum laser output. It can be seen from Fig. 3 that these mode jumps occur frequently and that they do have an effect on the observed powers and sidelight emission. The effect is relatively small in Fig. 3 ; however, in other experimental runs the effect was not tolerable. The basic problem was in finding the preset position for the translator to jump to; the position appeared to change from run to run. Between the mode jumps, the pump laser appears to be very well stabilized. However, for some experimental conditions, all the necessary data can not be recorded in this time interval.

A second stabilization procedure utilized the power output of one laser line instead of the total laser power to signal adjustment of the translator. However, this method also exhibited mode jump effects, with no significant improvement over broad-band lock-on.

The final solution was to operate the translator in the "fast sweep" manner. In the fast sweep, the translator moves through its full extension at a frequency of 5 Hz. In this way the observed data is seen to have an averaged stability. Figure 4 shows the total laser output power (a), the output power

of one laser line (b), and the cell sidelight emission at a given wavelength (c), with and without the translator operated in the fast sweep manner.

Section 4
CO - Ar V-T RATE MEASUREMENTS

4.1 MEASUREMENT OF CO VIBRATIONAL POPULATION DISTRIBUTIONS

The present experiments have extended the CO-Ar V-T rate data over a much wider range of vibrational quantum numbers; the range now extends from v = 10 to v = 42. This has been accomplished by varying the cell pressure from 1.0 to 23.5 atmospheres. A set of four experimental conditions spanning this range was chosen. To accomplish the pressure change an orifice downstream of the cell was restricted until the desired pressure was achieved. With the mass flows of CO and Ar fixed, the gas flow velocity changed to accommodate this pressure change. Table 2 lists the pump laser operating conditions and cell conditions for the four cases. In each case the CO 1st overtone infrared sidelight emission was recorded at a station 6 cm from the gas inlet port using the optical instrumentation outlined in Section 2. Figure 5 shows these spectra with case I the lowest pressure run and case IV the highest pressure run. The approximate center of selected vibrational band components is indicated on the figure.

Vibrational population distributions are inferred by comparison of the experimental spectra of Fig. 5 with computer-generated spectra, calculated using the same instrument response as the laboratory equipment. This spectrum is calculated for the experimental rotational-translational temperature (300°K), and for a vibrational quantum state population distribution chosen for the best fit to the experimental spectrum. A detailed description of this by-now-standard method of inferring vibrational populations from partially resolved spectra is given by Oettinger and Horn and outlined in last year's Interim Scientific Report.[1] It will be noted that inputs to the computed spectra, in addition to the vibrational populations N_v and the translational-rotational temperature T, include the usual molecular spectroscopic constants for the CO molecule, and the spontaneous emission "A" coefficients for all significantly intense transitions in the spectral range of interest. In the present work, the CO molecular spectroscopic constants of Mantz[4] and Roh and Rao[5] are used while the "A" coefficients used are based on the model calculations of Young and Eachus,[6] as extended by Fisher.[7] It should be noted that the significantly intense

TABLE 2

OPERATING CONDITIONS FOR SERIES OF CO-Ar V-T RATE MEASUREMENTS

Run No.	I	II	III	IV
Cell Pressure, atm	1.0	5.2	10.7	23.5
CO Concentration, cm^{-3}	1.97×10^{17}	1.02×10^{18}	2.10×10^{18}	4.62×10^{18}
Ar Concentration, cm^{-3}	2.28×10^{19}	1.17×10^{20}	2.43×10^{20}	5.34×10^{20}
Cell Gas Flow Velocity, cm sec^{-1}	965	187	90.5	41.1
Laser Power, watts	220	220	220	220
Laser Power Absorbed, watts	50	43	48	55

transitions for cases with measurable population of vibrational quantum states up to $V \approx 40$, include a substantial contribution of the 2nd overtone ($\Delta V=3$) transitions to the total spectrum in the 2.3 to 2.9 micron region.

Figure 6 shows the vibrational population distributions inferred using the synthetic spectrum method from the spectra of Figure 5. Referring to Figure 6, it will be noted that the distribution functions can be characterized by three regions of radically differing slopes. In the first region, below $V \approx 10$, the distribution initially falls rapidly from V=0. From the initial slope of the distribution in this region, a vibrational "temperature" can be inferred which is of the order of 2500°K. The initial slope decreases, entering a second, or "plateau" region, for $V \geq 10$. In the plateau region, the slope is relatively small, the decrease in population with increasing vibrational quantum number being slight. The quantum number at the end of the plateau region is a function of the partial pressures of the gas mixture. Beyond the plateau region, there is again a region of rapid falloff. The slope of the distribution in this region asymptotes to a value for which the inferred vibrational "temperature" is near the gas translational-rotational temperature, a Boltzmann distribution.

The kinetic processes governing the establishment of such "V-V pumped" distributions as those of Figure 6 are now well understood. The most recent systematic analysis is that of Lam[8]; the results of this work are used in the reduction of the present data. It has been shown that V-V pumped population distributions are created among the vibrational quantum levels of a diatomic gas whenever: (1) the rate of vibration-to-vibration (V-V) energy exchange upon collision of the diatomic molecules greatly exceeds the rate of energy addition into the vibrational mode, and (2) the specific internal energy in the rotational and translational modes is much less than the specific internal energy of the vibrational mode. With such a distribution established, it is shown in Reference 8 that the shape of the distribution in Region 1 is entirely determined by nonresonant V-V processes involving collisions of CO molecules in an excited vibrational state v with ground state molecules, i.e., inelastic processes between v=0 and v=n molecules causing simultaneous $v=0 \rightarrow 1$ and $v=n \rightarrow n-1$ transitions. In the plateau region, 2, the distribution is largely determined by resonant V-V processes, i.e., inelastic collisions involving simultaneous

$v=n \rightarrow n-1$ and $v=n-1 \rightarrow n$ transitions. Finally, the steep-slope Region 3 is controlled by V-T processes, i.e., direct collisional quenching of CO molecules in transition $v=n \rightarrow n-1$, not involving exchange of energy with other diatomic molecules. At the low concentrations of CO used in the present experiments, such V-T processes are controlled by collisions with the Ar diluent, V-T self-quenching by CO itself being negligible.

4.2 REDUCTION OF CO - Ar V-T RATES

The four distribution functions shown in Figure 6 can be predicted analytically as functions of the specific reaction rates for the V-V and V-T processes involved. Following Reference 8, the specific single-quantum-jump VT rate of $i+1 \rightarrow i$ collisions between CO and a diluent molecule M(M = Ar) can be written as:

$$k^{VT}(i+1 \rightarrow i) = \omega^{VT}_{CO-M}(T)\, l_i^{VT} (A_i^{VT})_M \,, \tag{4-1}$$

and the specific single-quantum jump V-V rate of $i \rightarrow i+1$, $j+1 \rightarrow j$ collisions between two CO molecules is:

$$k^{VV}(i \rightarrow i+1,\ j+1 \rightarrow j) = \omega^{VV}(T)\, l_i^{VV}\, l_j^{VV}\, A_{ij}^{VV}(T) \tag{4-2}$$

Here,

l_i^{VT}, l_i^{VV} are proportional to the square of the appropriate matrix elements and A_i^{VT} and A_{ij}^{VV} are the "adiabaticity" factors, terms having an exponential dependence on the quantum numbers involved in the transition. We assume

$$l_i^{VT} = \frac{1+i}{1-(.00598)i} \tag{4-3}$$

$$l_i^{VV} = \frac{1+i}{1+(.00897)i} \tag{4-4}$$

Still following the results of Lam et al., if one writes the V-T adiabaticity factor as

$$(A_i^{VT})_{Ar} \equiv B_r^{Ar} \exp \beta_{Ar}(i-r) \tag{4-5}$$

it can be shown that the distribution function in Regions II and III is expressed as

$$N_i = \frac{1}{\ell_i^{VV}} \left\{ N_r \ell_r^{VV} - N_{Ar}(C_{Ar})_r \left[\frac{e^{\beta_{Ar}(i-r)} - 1}{1 - e^{-\beta_{Ar}}} \right] \right\} \tag{4-6}$$

Here,

N_i = population of the i^{th} vibrational quantum level, [molecules cm^{-3}].

N_r = population of a selected reference vibrational quantum level, r, [molecules cm^{-3}].

$$C_{Ar} \equiv \frac{B_r^{Ar} T \omega_{CO-Ar}^{VT} \ell_r^{VT}}{2 b q \omega^{VV} \ell_r^{VV}} \tag{4-7}$$

$$b \equiv \frac{1}{2} \sum_{j=0}^{\infty} (i-j)^2 A_{ij}^{VV}(T) \exp [(\Delta E_i - \Delta E_j)/2kT] \tag{4-8}$$

b is essentially the second moment of the V-V rate adiabaticity factors. It is shown in Reference 8 that this parameter is essentially independent of i. Using recent data of Brechignac,[9] it is shown that this parameter can be scaled as a simple function of temperature:

$$b \cong 6.6\left(\frac{T}{150}\right)^{3/2}$$

q = $2\omega_e x_e / k$, where $\omega_e x_e$ is the CO anharmonicity

= 37°K.

ω_{vv} = 1.26×10^{-12} cm^3 sec^{-1} molecule^{-1}, as determined by matching 300°K data of Reference 10, using procedure of Reference 9. (4-9)

From Equations (4-1), (4-5) and (4-7), it can be shown that the V-T rates can be rewritten as

$$k^{VT}(i+1 \rightarrow i) = \frac{2bq\omega^{VV} l_r^{VV}}{T l_r^{VT}} (C_M)_r \, l_i^{VT} \exp \beta_M (i-r) \qquad (4\text{-}10)$$

If the reference level V=r were chosen at the beginning of the plateau region, it can be shown that only the last two terms in the distribution function, Equation (4-6), are dependent on the V-T rates. Then for states v=i in the beginning of the plateau region, these V-T dependent terms are negligible, and $N_i \approx \frac{l_r^{VV}}{l_i^{VV}} N_r$; this distribution can be considered the zeroeth approximation to the shape of the V-V pumped plateau, and, noting the quantum number dependence of l_i^{VV} , shows the product iN_i is approximately constant in this region, a result first noted by Center and Caledonia.[11] Farther into the plateau, the V-T quenching terms in Equation (4-6) begin to be significant, resulting in a steeper slope, and finally, creating a "knee" in the distribution which ends the plateau.

Fitting the predicted distribution function, Equation (4-6), to the measured distributions permits the V-T rates of the form (4-10) to be inferred. The fitting procedure is as follows. A reference level r is selected, and N_r chosen to equal the experimentally measured population for this quantum level.*

*The reference level chosen in the actual fitting procedure is not at the beginning of the plateau region, but well into the region of the distribution where V-T effects are significant.

The remaining undetermined constants C_{Ar} and β_{Ar} in the rate expression, Equation (4-10), are then chosen by trial and error to give the best fit of Equation (4-6) to the measured distribution in Region 2. The results of this procedure are shown in Figures 7 - 10 for each of the four cases. The measured distribution is plotted, together with the best fit of the analytical distribution Equation (4-6). It can be seen that the fit to the experimental distribution in the plateau region, Region 2, is quite good. Since Equation (4-6) applies only to Region 2, the fit in Regions 1 and 3 is not critical to the rate reduction. The experimental distribution in Case III shows an anomalously slow fall off in Region 3, whereas the other cases show fair agreement even in this region.

In each case, the rate expression reduced has maximum sensitivity to the fit parameters at the boundary of Regions 2 and 3. Thus in the vibrational quantum number range about this boundary is where each case will yield an accurate V-T rate measurement. Figure 11 shows the rates reduced for five vibrational levels from each case that lie near the boundary of Regions 2 and 3. The reduced rates are shown as points; the solid curve is an exponential fit to these reduced rates. It must be emphasized that the exponential fit has an experimental basis only in the range $V \approx 10$ to $V \approx 42$. The rate is plotted as a dimensionless transition probability, $P_{v,v-1}$, for the $v \rightarrow v-1$ transition, versus vibrational quantum number, V. The "transition probability", $P_{v,v-1}$, is related to the specific V-T rate k^{VT} $(v + 1 \rightarrow v)$ of Equation (4-10) by the collision frequency Z,

$$k^{VT}(V \rightarrow V-1) = Z P_{v,v-1}$$

where

Z = collision frequency in units of $cm^3\ sec^{-1}\ molecule^{-1}$

$$Z = 4\sigma^2 \sqrt{\frac{\pi k T}{2\mu}}$$

σ = molecular hard sphere diameter

μ = reduced mass of collision partners

In this report

$$\Xi \text{ CO-Ar } (300^{\circ}\text{K}) = 2.664 \times 10^{-10} \text{ cm}^3 \text{ sec}^{-1} \text{ molecule}^{-1}$$

The inferred CO-Ar V-T rate expression, as plotted as the solid curve in Figure 11, is given by

$$k^{VT}_{\text{CO-Ar}} (V + 1 \rightarrow V) = 1.34 \times 10^{-19} \; l^{VT}_{v} \; e^{0.13V} \text{ cm}^3 \text{ sec}^{-1} \text{ molecule}^{-1}$$

Section 5
COMPUTER MODELING OF CELL KINETICS

Under a related USAF contract, a kinetic model and computer code has been developed[12] which can be used for analysis of the optically-pumped-cell experiments of the present program. A full description of the model and code is given in Ref. 12; its major features are briefly summarized here for completeness.

The model describes the optical pumping of the vibrational distribution by the absorption of the incident laser radiation, collisional pumping by vibration-vibration (V-V) energy exchange collisions, and losses due to vibration-translation (V-T) energy exchange collisions and to spontaneous radiative transitions. The incident laser beam is directed along the axis of the high-pressure cell, which is also the flow direction of the gases in the cell. The primary assumptions made in the model are:

(1) The flow in the cell and the radiative absorption process are one-dimensional, i.e., the flow properties, population distributions, and radiative intensities are constant over a cross-section normal to the beam/flow direction.

(2) The incident laser lines have a much smaller linewidth than the absorption lines in the cell.

(3) The individual vibrational-level populations depart from equilibrium due to the radiative and collisional processes, but the rotational state populations within each vibrational level remain in equilibrium with the translational temperature.

First, the radiative transport equations are given for the variation through the cell of the intensities of the pumping laser lines. If at axial position x, the spectrally integrated intensity of the j^{th} laser line (in watts/cm^2) is $I_{\nu_j}(x)$, the radiative transport equation for each line intensity is written

$$\frac{dI_{\nu_j}}{dx} = \alpha_{\nu_j} I_{\nu_j} \qquad (5\text{-}1)$$

where α_{ν_j} is the net gain coefficient in cm^{-1} (α_{ν_j} is defined to be negative when the gas is in absorption at ν_j). The gain coefficient expression is used which accounts for the overlapping of the pressure-broadened vibration-rotation lines. The spontaneous emission or source term has been dropped from this equation because spontaneous emission, which is isotropic, is not expected to be important in the specific direction of I_{ν_j} .

In addition to the equations for the radiative intensities, the kinetics equations for the vibrational level populations are required. Since the cell kinetics computer program has been based on the Calspan CO flow-laser kinetics code,[13,14] the master equations for the vibrational level populations have been written in the same form as used there, with suitable modification of the stimulated emission and absorption terms. The concentration of molecules in the V^{th} level, in moles per gram of mixture, γ_v , satisfies

$$u \frac{d\gamma_v}{dx} = C_v^{v-T} + C_v^{v-v} + \psi_{v+1,v} - \psi_{v,v-1} \qquad (5\text{-}2)$$

$$+ A_{v+2,v}\gamma_{v+2} + A_{v+1,v}\gamma_{v+1} - (A_{v,v-2} + A_{v,v-1})\gamma_v$$

where u is the flow velocity, C_v^{v-T} and C_v^{v-v} are the rates of production of molecules in level V due to V-T and V-V collisions, $A_{v',v}\gamma_{v'}$, represents the spontaneous emission terms, and $\psi_{v',v}$ is the net production rate for level V by stimulated emission and absorption transitions between levels V and V'. The stimulated emission and asbsorption rates are written in terms of the intensities and the absorption coefficients for individual vibrational-rotational transitions. The detailed descriptions of the V-T and V-V rate models are given in References 13 and 14.

These coupled equations for the line intensities and vibrational level populations are integrated together with the gasdynamics equations for one-dimensional flow. The form of the equations for the gasdynamic variables are

as given in References 13 and 14, specialized to a constant cross-sectional area of the flow channel; the method of numerically integrating the equations is presented there also.

Given initial gas properties, an initial vibrational population distribution, the initial intensities and the frequencies of the incident laser lines, the above equations can be integrated to find the variation of these quantities along the cell. The V-V, V-T, and radiative rates that are used in the calculation are all-important in determining the vibrational distribution function at various axial positions. Previous calculations using this code did not have available the CO-He and CO-Ar rates measured in the present program. These previous calculations accordingly used the sparse earlier CO-He data,[1] and used very crude approximations for the CO-Ar rates, since no experimental values were available.

Using the newly-determined CO-Ar rates as given in Fig. 11, we have performed a series of calculations with the modeling code. These new calculations have been made to verify that vibrational distribution functions are produced that are similar to those determined by experiment, thus providing a cross-check on the analytical theory of Ref. 8 used in the data reduction. In addition, the validity of certain key assumptions made in the data reduction process can be examined in detail.

One of the limitations of the computer code, as presently set up, is that it does not model the "triggering" process, which establishes the initial absorption of pump radiation. (This triggering process is briefly discussed in Section 2.2.3 above.) Without incorporation of this triggering feature, absorption of pump radiation is slow, and an unrealisticly long length of the cell is required before pumped distributions comparable to those of Fig. 6 are produced. In the actual experiments, the triggering processes discussed in Section 2.2.3, combined with streamwise radiative coupling on the optically thick CO fundamental band IR transitions, result in production of vibrationally excited CO within the two centimeters of cell length. For the range of flow velocities and concentrations of the experiments summarized in Fig. 6 and

Table 2, V-V pumping is sufficiently rapid to create a fully developed plateau-pumped distribution within this same ~ 2 cm of cell length. Experimental monitoring of the IR emission from various axial stations confirms that these quasi-steady state distributions are maintained along the subsequent length of the cell. In order to simulate this triggering effect, all computer runs were started, at the upstream x = 0 axial station, with an initial vibrational distribution equal to Case I of Fig. 6. As will be shown, for all cases run, the vibrational population distribution adjusted to a quasi-steady value determined by the particular run parameters selected.

Figures 12 to 14 show the results of these model calculations, using the new CO-Ar rates of Fig. 11. Three runs were made using the parameters of the CO-Ar experimental Cases I through III of Table 2. Note that the basic parameter varied among these three cases is the total gas pressure, going from 1.0 atm in Case I to 10.7 atm in Case III. The CO/Ar mole fraction remains approximately constant. As noted above, all three runs commenced with an initial vibrational population distribution given by the plot of Case I, Fig. 6. Initial cell temperature was 300°K, and the pump laser spectral distribution was as given in Table 3.

Figure 12 is a plot of the calculated vibrational energy as a function of distance along the cell axis for the three cases. Initial vibrational energy is 0.308 eV per CO molecule; since the calculation commenced with a population distribution determined experimentally to be the quasi-steady state for the parameters of Case I, the vibrational energy remains very nearly constant for this case. For the two higher pressure cases, II and III, the vibrational energy quickly falls, establishing new, lower, quasi-steady values within 2 cm. The quasi-steady values are maintained by the balance between energy input via absorption of pump laser radiation, and losses via radiative, V-V, and V-T processes. As the gas pressure increases, the V-T loss rate increases, resulting in the lowering of the quasi-steady vibrational energy shown in Fig. 12.

Figure 13 shows the quasi-steady distribution functions at the x = 4.0 cm station in the cell, for the same three cases. These distributions are established

TABLE 3

LASER SPECTRUM AT 15% OUTPUT COUPLING;
ROOM TEMPERATURE OPERATION

Vibrational Band	Rotational Line	Wavelength, μ	% Total Power
V = 3 - 2	P(7)	4.84679	2.90
	P(8)	4.85624	1.88
V = 4 - 3	P(5)	4.89001	0.84
	P(6)	4.89939	6.42
	P(7)	4.90888	6.04
	P(8)	4.91849	1.01
V = 5 - 4	P(5)	4.95323	1.76
	P(6)	4.96277	5.63
	P(7)	4.97242	5.10
V = 6 - 5	P(5)	5.01793	6.30
	P(6)	5.02763	9.05
	P(7)	5.03745	5.13
V = 7 - 6	P(4)	5.07441	0.59
	P(5)	5.08415	3.25
	P(6)	5.09401	4.53
	P(7)	5.10400	1.48
V = 8 - 7	P(4)	5.14205	1.19
	P(5)	5.15195	7.25
	P(6)	5.16198	2.88
	P(7)	5.17214	0.34
V = 9 - 8	P(4)	5.21129	4.31
	P(5)	5.22137	4.26
	P(6)	5.23158	1.07
	P(7)	5.24192	0.40

TABLE 3 (continued)

Vibrational Band	Rotational Line	Wavelength, μ	% Total Power
V = 10 - 9	P(3)	5.27209	2.80
	P(4)	5.28222	1.34
	P(5)	5.29247	1.94
V = 11 - 10	P(4)	5.35489	1.72
	P(5)	5.36533	4.35
	P(6)	5.37591	0.36
V = 12 - 11	P(4)	5.42933	1.37
	P(5)	5.43996	1.90
	P(6)	5.45073	0.66
V = 13 - 12	P(3)	5.49496	1.54
	P(4)	5.50565	0.53
	P(5)	5.51647	0.95
	P(6)	5.52744	0.39
V = 14 - 13	P(5)	5.59488	0.81
V = 15 - 14	P(4)	5.66407	0.60

before x = 2.0 cm, and persist downstream in the cell unless laser pump power is exhausted. As total gas pressure decreases, the V-V pumped plateau extends to higher quantum numbers. Figure 13 should be compared with the experimentally measured distributions of Fig. 6, inferred for the same operating conditions. It can be seen that the relative populations of the plateau regions and their extent are quite similar. The details of the shape of the plateaus and high-quantum-number fall-off regions differ; however, the agreement among the measured distributions, the machine-code calculation of Fig. 13, and the analytic results of Ref. 8, as plotted in Figs. 7 to 9, is sufficiently good to create confidence in the inferred CO-Ar V-T rates of Fig. 11.

Finally, Fig. 14 is a plot of the total pump laser power absorbed as a function of distance along the cell. For all cases, power is absorbed linearly with distance. Absorption is primarily by the lowest vibrational quantum states of the CO, below the plateau; since populations of these states do not change, even in the first 1-2 cm of the cell, the absorption rate remains constant. The total power that is absorbed in the 25 cm total cell length is of the order of the total absorptions observed experimentally for these conditions.

Section 6
STUDY OF V→E TRANSFER PROCESSES

6.1 GENERAL

In this section, we summarize the experimental evidence for transfer from the CO vibrational mode to the electronic modes of C_2 and CN molecules, obtained during the present program. These results have suggested a concept for a powerful visible-wavelength laser, based on molecular V→E transfer. During the course of the past year, some attention has been paid to analyzing the kinetics of the transfer process and assessing the potential for laser action on electronic bands by this mechanism. This work is reported in the following subsections.

6.2 SUMMARY OF EXPERIMENTAL RESULTS ON MOLECULAR ELECTRONIC FLUORESCENCE

As described in last year's report,[1] it was observed that the energy per CO molecule stored in the vibrational mode increases with decreasing total gas pressure in the absorption cell. At total gas pressures below approximately 6 atmospheres in CO/Ar mixtures, a visible blue emission is seen in the pumped gas, the intensity increasing as the pressure decreases. This glow is created by emission from the Swan bands of the C_2 molecule. Figure 15 shows the $\Delta V = 0$ sequence of these Swan bands ($A\,^3\Pi_g - X\,^3\Pi_u$ transitions). Additional sequences of these same bands were given in the figures of Ref. 1. It should be noted that the rotational fine structure of these bands is resolved; the relative intensity of these lines confirms that the rotational/translational temperature is maintained near 300°K.

In a separate series of experiments, mixtures of CO and N_2 in Ar diluent have been optically pumped in the cell. The N_2 vibrational states are in fairly close resonance with those of CO, and the N_2 is vibrationally excited by rapid V-V transfer from the pumped CO. At lower pressures, CN formation has been observed, strong emission from the CN violet bands being monitored. The CN emission initially increases with added nitrogen, until the diatomic molecule

concentration increases to the point where the energy loading of the vibrational modes is substantially lowered. Beyond this point, CN emission decreases as nitrogen is added.

Figures 16 and 17 show the $\Delta V = 0$ sequence of the CN violet bands. The spectrum of Fig. 16 was obtained for a 0.4% CO, 1.4% N_2, 98.2% Ar mixture at a total cell pressure of 350 torr and a flow velocity of 943 cm/sec. In addition to the $V = 0 \rightarrow 0$, $1 \rightarrow 1$, $2 \rightarrow 2$, $3 \rightarrow 3$, and $4 \rightarrow 4$ components of the CN $\Delta V = 0$ sequence, the $V = 0 \rightarrow 0$ and $1 \rightarrow 1$ components of the C_2 DesLandres-d'Azambuja bands are also seen. An interesting feature of these CN spectra is that the well-known P-branch band heads are not observed. This lack of heading is caused by the low rotational temperature of the CN (approximately 300°K). The P-branch band heads for the CN system occur at rotational quantum level J = 28; such high rotational levels are not populated at 300°K, and hence the head does not form. This feature is further illustrated in Figure 17 where the same CN violet $\Delta V = 0$ bands are shown. In the top trace, the unheaded bands are again shown, being created in the cell with a flow velocity of $\sim$1000 cm/sec. In the lower trace, the flow velocity had deliberately been slowed down drastically, allowing the translational/rotational temperature of the gas to rise. The band heads become immediately apparent. Again, it is apparent that rotational relaxation is occurring much more rapidly than the radiative decay time of the emitting electronic system, in this case, CN ($B^2\Sigma^+$).

6.3 DISCUSSION OF RESULTS

A major technical issue is the determination of the mechanism for the observed electronic excitation of C_2 and CN. In forming a working hypothesis, three principle experimental features should be noted:

i) There is no evidence of electronically excited CO. Unlike the visible emission from a CO laser electric discharge, there appears to be no emission from the CO Angstrom bands or other CO electronic states.

ii) Two of the observed electronic states of C_2 and CN (the $C_2\, C'\,{}^1\Pi_g$ and CN $B^2\Sigma^+$) have, respectively, an electronically excited C and N atom as one of their dissociation products.

iii) The C_2 and CN electronic states observed in emission to date have energies below many of the vibrational states observed in the optically pumped CO (cf. Table 1).

On the basis of these observations, it can be hypothesized that the C_2 and CN are formed in their ground electronic states and subsequently are electronically excited by energy transfer from the vibrational modes of CO (and N_2) during molecular collisions. It is difficult to see how the electronic excitation of C_2 and CN is accomplished otherwise. Optical pumping is by means of relatively low energy 5μ infrared photons; pump intensities are of the order of a few 100 watts/cm^2. Accordingly, there is little probability of direct multiphoton excitation of electronic states or multiphoton dissociation. This is supported by the lack of any observed CO excited electronic states. Further, the direct formation of C_2 and CN in the observed electronic states requires, for some of the transitions noted, the presence of electronically excited C or N atoms; it is difficult to see how these could be formed by direct optical excitation.

It is interesting to note that the hypothesized mechanism of vibrational-to-electronic transfer between molecules and subsequent strong visible emission from the excited electronic state is an example of a class of kinetic processes recently studied by Capelle and Sutton and used to measure the concentrations of very small amounts of gas phase trace species (Ref. 15). In terms of energy transfer in the CO-C_2 system, this kinetic mechanism can be written as:

$$CO(V \approx 11) + C_2(X'\Sigma_g^+)$$

$$\xrightarrow{k} CO(V=0) + C_2(A^3\Pi_g) \qquad (6\text{-}1)$$

$$C_2(A^3\Pi_g) \xrightarrow{1/\tau} C_2(X^3\Pi_u) + h\nu_{VISIBLE} \qquad (6\text{-}2)$$

Basically, this mechanism assumes that the vibrationally excited CO can be regarded as a metastable present in large excess, and that the radiative step, Reaction (6-2), is very rapid ($10^{-8} \leq \tau \leq 10^{-6}$ sec.). These conditions, although developed in Ref. (15) to interpret experiments with quite different species, are met by the slow-relaxing vibrational mode of CO and the large f numbers of the C_2 Swan transitions; these transitions have radiative lifetimes of $\sim 1 \times 10^{-6}$ sec. For typical conditions of our experiment, the average time between collisions of C_2 with vibrationally excited CO is more than an order of magnitude longer than these radiative lifetimes. With such time scales, and in the absence of rapid collisional quenching, essentially every C_2 ($A^3\Pi_g$) formed by Reaction (6-1) undergoes rapid radiative decay via Reaction (6-2), and pseudo first-order kinetics obtain, with Reaction (6-1) the rate-limiting step. It can be shown that the emitted visible fluorescence intensity on the C_2 Swan is then given by:

$$I = k[CO(V \gtrsim 11)][C_2(x'\Sigma_g^+)] \qquad (6\text{-}3)$$

Accordingly, the intensity of emission from the C_2 Swan bands is proportional to the amount of vibrationally excited CO. Strong emission is possible from very small amounts of C_2, provided large quantities of CO ($V \approx 11$) are present.

6.4 V ⟶ E TRANSFER LASER CONCEPT

Under the stated conditions producing the C_2 fluorescence, as analyzed in the preceding subsection, no partial population inversion or subsequent gain can be expected on the C_2 Swan vibronic bands. Even if gain were sought on transitions whose lower state was a relatively high-lying vibrational level of C_2 ($x'\Sigma_g^+$), the extremely rapid radiative depopulation of the upper C_2 ($A^3\Pi_g$) level would preclude any population inversion.

It is possible, however, to conceive of molecular V ⟶ E transfer systems, based on highly vibrationally excited CO, which can produce significant partial populations on vibronic bands. In this more general concept, the emission described by Eqs. (6-1)-(6-2) is a (rather unfavorable) limiting case. For simplicity

in this short outline, we will consider only a diatomic molecule "A_2" possessing two electronic states, $A^1{}_2$ and $A^2{}_2$, with $E_1 > E_2$; electronic state 2 need not be the molecular ground state. We are interested in the possibility of creating optical gain on transitions between some rotational substate of the m^{th} vibrational state of $A^1{}_2$, and another rotational substate of the n^{th} vibrational state of $A^2{}_2$, i.e., gain on a transition:

$$A_2'(V = m, J') \longrightarrow A_2^2(V = n, J'')$$

The upper state, A_2^1 (v = m), is excited by collisional V → E transfer from the vibrationally excited CO. In principle, there can be many vibrational states of the lower electronic level of A_2 which can accept vibrational energy from CO and be excited to the A_2^1 (v = m) state. Similarly, there can be many vibrational states of CO having sufficient energy to cause such a transition during an inelastic V → E transfer collision. For the purposes of the present discussion, however, it will be assumed that only a single V-E energy transfer channel is open, i.e., only two pairs of states participate in the transfer process. Figure 18 is a sketch of this simplest situation. In the figure, the potential curve on the left is that of the CO molecule; on the right are the potential curves for the A_2^1 and A_2^2 states of the A_2 molecule. The energy exchange channel under consideration is a collision of CO in level V = i with A_2^2 (v = n), with consequent collision-induced transitions v = i → j in CO and A_2^2 (v - n) → A_2^1 (v = m) in A_2. As sketched in the figure, this V → E exchange transition is nearly a resonant process, with a very small energy defect; in practice, it has been noted that the resonant channel is not always dominant in all V → E exchange processes.[16] The nature of the argument here, however, is not dependent on near-resonant exchange.

Using the model described above, we consider the processes controlling the population of A_2^1 (v = m), namely, V → E exchange with CO, radiative decay, and direct collisional quenching, and write a rate equation governing the population of this state:

$$\frac{d[A_2(V=m)]}{dt} = k_{n\to m}^{V\to E}\left[CO(V=i)\right]\left[A_2^2(V=n)\right] - k_{m\to n}^{E\to V}\left[CO(V=j)\right]\left[A_2^1(V=m)\right] - \frac{1}{\tau_{RAD}}\left[A_2(V=m)\right] - k_{QUENCH}\left[M\right]\left[A_2^1(V=m)\right] \quad (6\text{-}4)$$

Here, the brackets indicate concentrations in molecules/cm^3. $k_{n\to m}^{V\to E}$ and $k_{m\to n}^{E\to V}$ are the forward and reverse specific V-E rate constants for the indicated exchange transition, τ_{RAD} is the radiative lifetime of the A_2^1 (v = m) state, and k_{QUENCH} is the specific rate for the collisional quenching of the A_2^1 (v = m) state by collisions with diluent species M. Naturally, if other V-E channels are open, as discussed above, or if there is more than one effective quenching species, the single terms in Eq. (6-4) will be replaced by sums over states and species.

Equation (6-4) can be solved for the ratio of upper to lower level populations, $[A_2^1$ (v = m)] / $[A_2^2$ (v = n)], by setting d$[A_2^1$ (v = m)]/dt equal to zero, with the result:

$$\frac{\left[A_2^1(V=m)\right]}{\left[A_2^2(V=n)\right]} = \frac{k_{n\to m}^{V\to E}\left[CO(V=i)\right]}{k_{m\to n}^{E\to V}\left[CO(V=j)\right] + \frac{1}{\tau_{RAD}} + k_{QUENCH}\left[M\right]} \quad (6\text{-}5)$$

Two limiting cases of the above result can be recognized:

I Rapid Fluorescence:

For this case,

$$\frac{1}{\tau_{RAD}} >> k_{m\to n}^{E\to V}\left[CO(V=j)\right], \quad (6\text{-}6)$$

i.e., every A_2 molecule that is electronically excited by collision with vibrationally excited CO is almost immediately deactivated by rapid spontaneous emission (or collisional quenching). In this limit, the emitted spontaneous fluorescence intensity, $I_{FLUORESCENCE}$ is given by:

$$I_{FLUORESCENCE} = \frac{1}{\tau_{RAD}} \left[A_2' (V = m) \right]$$

$$\approx \frac{k_{n \to m}^{V \to E} \left[CO (V = i) \right] \left[A_2 (V = n) \right]}{1 + \tau_{RAD} / \tau_{QUENCH}} \qquad (6\text{-}7)$$

where $\tau_{QUENCH} \equiv \left[k_{QUENCH} [M] \right]$

It can be recognized that for $\tau_{RAD} / \tau_{QUENCH} << 1$, this result is identical to Eq. (6-3) given previously; this limiting case is an approximation to the actual conditions in our apparatus which create the C_2 Swan band fluorescence shown in Fig. 15.

II V-E Quasiequilibrium Limit:

For this case,

$$\frac{1}{\tau_{RAD}} << k_{m \to n}^{E \to V} \left[CO (V = j) \right] \qquad (6\text{-}8)$$

and therefore Eq. (6-5) yields:

$$\frac{\left[A_2' (V = m) \right]}{\left[A_2^2 (V = n) \right]} \cong \frac{k_{n \to m}^{V \to E} \left[CO (V = i) \right]}{k_{m \to n}^{E \to V} \left[CO (V = j) \right] + \tau_{QUENCH}^{-1}} \qquad (6\text{-}9)$$

For cases where the E $\rightarrow$ V energy exchange transitions are in exact resonance, $k_{n \to m}^{V \to E} / k_{m \to n}^{E \to V} = 1$, by detailed balance. If τ_{QUENCH} is then very long, it can be seen that Eq. (6-9) implies the electronic level populations are in equilibrium with vibrational population distribution of the CO.

Conditions approaching the limit given in Case II are, of course, desirable for V → E transition laser potential. In this limit, the electronic levels can be in a "partial population inversion" similar to those of the CO vibrational states, and gain can be realized on some P-branch vibronic transitions, the small signal gain expression being similar to that originally derived by Patel[17] for vibrational bands:

$$\alpha = \frac{\text{CONSTANT}}{\tau_{RAD}} \left\{ \left[A_2^1 (V = m) \right] B_{1,m} e^{-E_{J'}/kT} - \left[A_2^2 (V = n) \right] B_{2,n} e^{-E_{J''}/kT} \right\} \qquad (6\text{-}10)$$

Here, α is the small signal gain on the J' → J'' rotational line of the A_2^1 (V = m) → A_2^2 (V = n) vibronic transition, $B_{1,m}$, $B_{2,n}$ and $E_{J'}$, $E_{J''}$ are the rotational spectroscopic constants and the rotational energies, respectively, for the indicated states.

On the basis of Eqs. (6-8)-(6-10), criteria for realizing useful gain in a molecular V → E transfer system can be stated. It should just be noted that the partial inversion $[A_2^1 (V = m)] / [A_2^2 (V = n)]$, when substituted in the gain expression Eq. (6-10), will at best yield only inversions comparable to those in the CO V-V pumped "plateau" as shown in Fig. 6. To obtain useable gain on transitions at visible wavelengths, τ_{RAD} must be much shorter than the lifetimes for vibrational laser transitions. This is, of course, generally the case; the infrared lifetimes are measured in milliseconds, the electronic lifetimes are orders of magnitude shorter. This feature will allow rather weak partial inversions to yield gain (as per Eq. (6-10)) on electronic transitions, when the corresponding gain on a vibrational transition (such as a high-overtone transition in CO itself) would be prohibitively small. Nevertheless, the radiative lifetime cannot be so short as to violate (Eq. (6-3); as we have seen, very large radiative f numbers result in rapid fluorescence decay, i.e., limiting Case I. Given, however, a radiative lifetime that indicates useable gain (via Eq. (6-10)), criterion (6-8) can be satisfied if a sufficient amount of vibrationally excited CO is present. It is also apparent from Eq. (6-8) that the E → V specific rate

constant, $\ell^{E\to V}_{m\to n}$ must be known for each candidate molecular system before its laser potential can be quantitatively assessed. Finally, it should be noted that it may be possible to choose transitions for which there is a considerable disparity in the rotational spectroscopic constants $B_{1,m}$, $B_{2,n}$ with a corresponding difference in the rotational energies $E_{J'} \equiv B_{1,m} J'(J'+1)$, $E_{J''} \equiv B_{2,n} J''(J''+1)$. Transitions for which $B_{1,m} << B_{2,n}$ will generally have higher small signal gain.

The preceding considerations can be enumerated in a list of criteria for a suitable molecule to be used in an electronic band laser being excited by V→E transfer from vibrationally-pumped CO:

1. The molecule must not be a fast V-T relaxant for CO. In all analysis, it is assumed the lasant species does not significantly quench the excited CO via V-T collisions.

2. The rate of E-V transfer from CO must be sufficiently fast to allow Eq. (6-8) to be satisfied for realizable concentrations of vibrationally-excited CO.

3. The radiative lifetime of the electronic transition must not be so long as to preclude useable gain being obtained on partial inversion transitions (Eq. (6-10).

4. The electronic transition chosen must yield gain at a desirable visible or UV wavelength.

5. The energies of both the upper and lower laser levels must lie within the range of the V-V pumped "plateau" of Fig. 6, i.e., 2.5 eV $\lesssim E_1, E_2$ 7.5 eV. This criterion does not entirely preclude use of an electronic transition terminating in the ground electronic state; however, for such a case, the vibrational level of the lower state must be above $\sim$ 2.5 eV.

6. Transitions for which $B_{v''} > B_{v'}$ will generally be advantageous, unless the Franck-Condon factors are extremely unfavorable.

Candidate Transfer Species

On the basis of the preceding criteria, a systematic search of molecular spectral and lifetime data can be made to identify likely candidate transfer species. For such systems, detailed kinetic estimates and gain calculations can be made. V - E transfer rate measurements can then be made for the more promising systems; the details of the proposed experimental program are given in the following section.

At the present time, such a detailed search procedure has not been performed. However, estimates have been made for a few of the more common diatomic electronic bands satisfying the above criteria. Two such systems, the NO β and the CN $D^2\pi_i \rightarrow A^2\pi_i$ are sufficiently promising to warrant further study. For high concentrations of vibrationally excited CO, it appears that a V - E quasiequilibrium can be established with these systems, if the V - E transfer rate is sufficiently rapid. Figure 19 gives a plot of the small signal gain (Eq. (6-10)) to be expected from the NO β system when such an equilibrium is established. It should be re-emphasized that an extensive screening of molecular systems should produce additional candidate systems.

REFERENCES

1. Rich, J.W., Bergman, R.C., and Williams, M.J., "Measurement of Kinetic Rates for Carbon Monoxide Laser Systems", Interim Scientific Report AFOSR Contract No. F49620-77-C-0020, Calspan Corporation Report No. WG-6021-A-1, November 1977.

2. Treanor, C.E., Rich, J.W., and Rehm, R.G., J. Chem. Phys. 48, 1798 (1968).

3. Milliken, R.C., J. Chem. Phys. 38, 2855 (1963).

4. Mantz, A.W., Nichols, E.R., Alpert, B.D. and Rao, K.N., Journal of Molecular Spectroscopy 35, 325-328, (1970).

5. Roh, W.B. and Rao, K.N., J. Mol. Spectrosc. 49, 317 (1974).

6. Young, L.A. and Eachus, W.J., J. Chem. Phys. 44, 4195 (1966).

7. Lightman, A.J. and Fisher, E.R., Appl. Phys. Lett. 29, 593 (1976); Fisher, E.R., Private Communication (1977).

8. Lam, S.H., J. Chem. Phys. 67, 2577 (1977).

9. Brechignac, P., "Near Resonant UV Transfer Rates for High-Lying States of Diatomic Gases", Private Communication, Submitted to J. Chem. Phys. (1977).

10. Powell, H.T., J. Chem. Phys. 59, 4937 (1973).

11. Caledonia, G.E. and Center, R., J. Chem. Phys. 55, 552 (1971).

12. Lordi, J.A., and Rich, J.W., "A Theoretical Study of a High-Pressure, Tunable CO Laser", Report No. AFAL-TR-75-184, USAF Avionics Laboratory, December 1975.

13. Lordi, J.A., Falk, T.J., and Rich, J.W., "Analytical Studies of the Kinetics of Electrically Excited, Continuously Operating CO Flow Lasers", AIAA Paper No. 74-563, AIAA 7th Fluid and Plasma Dynamics Conference, Palo Alto, California, June 17-19, 1974.

14. Rich, J.W., Lordi, J.A., Gibson, R.A. and Kang, S.W., "Supersonic Electrically Excited Laser Development", Calspan Report No. WG-5164-A-3, June 1974.

15. Capelle, G.A., and Sutton, D.G., "Analytical Photon Catalysis: Measurement of Bi Concentrations to $10^4/cm^3$", Aerospace Corporation Report No. SAMSO-TR-77-96, 19 April 1977.

16. Lemont, S., and Flynn, G.W., Ann. Rev. Phys. Chem. 28, 261 (1972).

17. Patel, C.K.N., Phys. Rev. Lett. 12, 588 (1964).

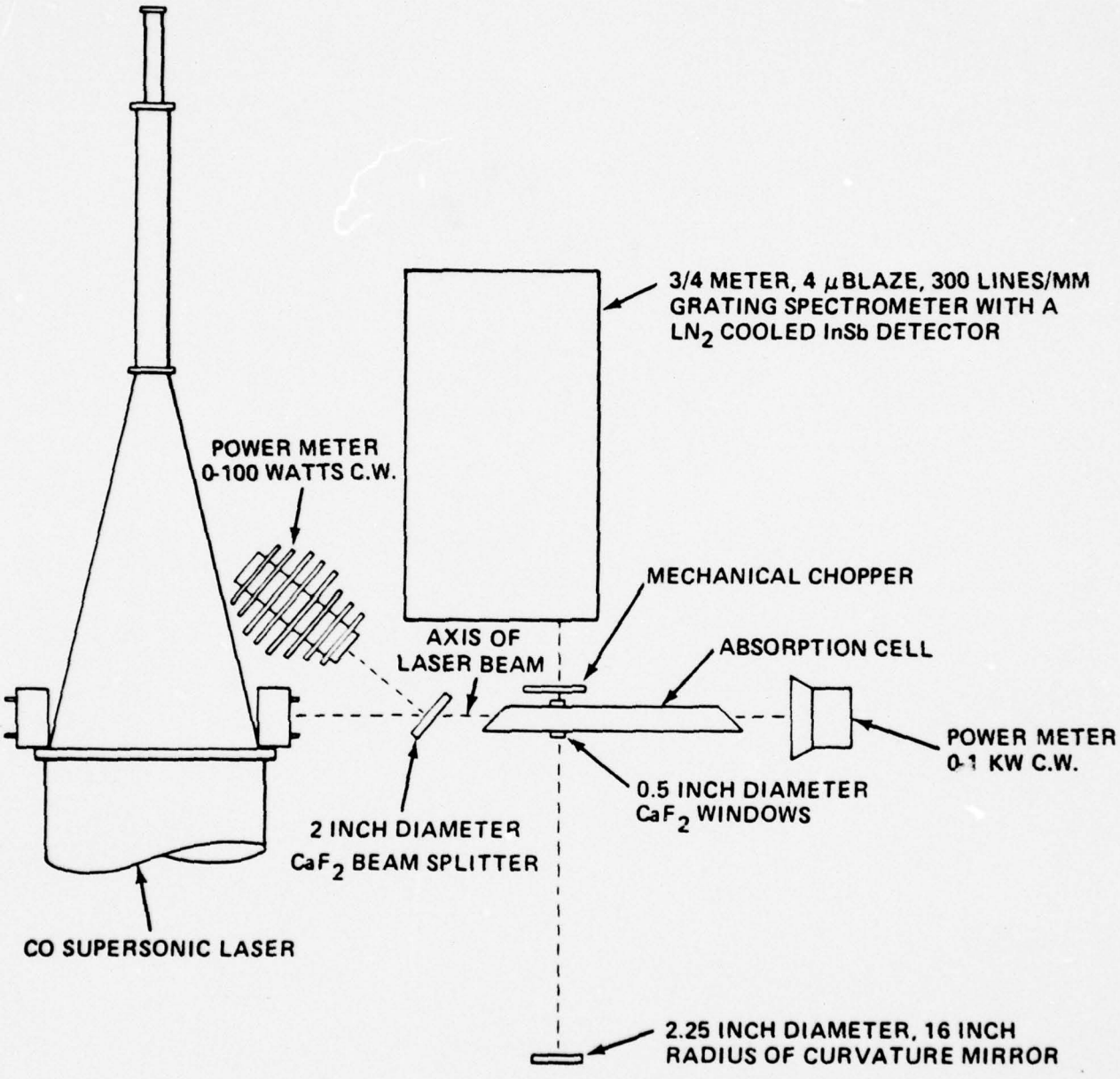

Figure 1 SCHEMATIC OF OPTICAL PUMPING APPARATUS

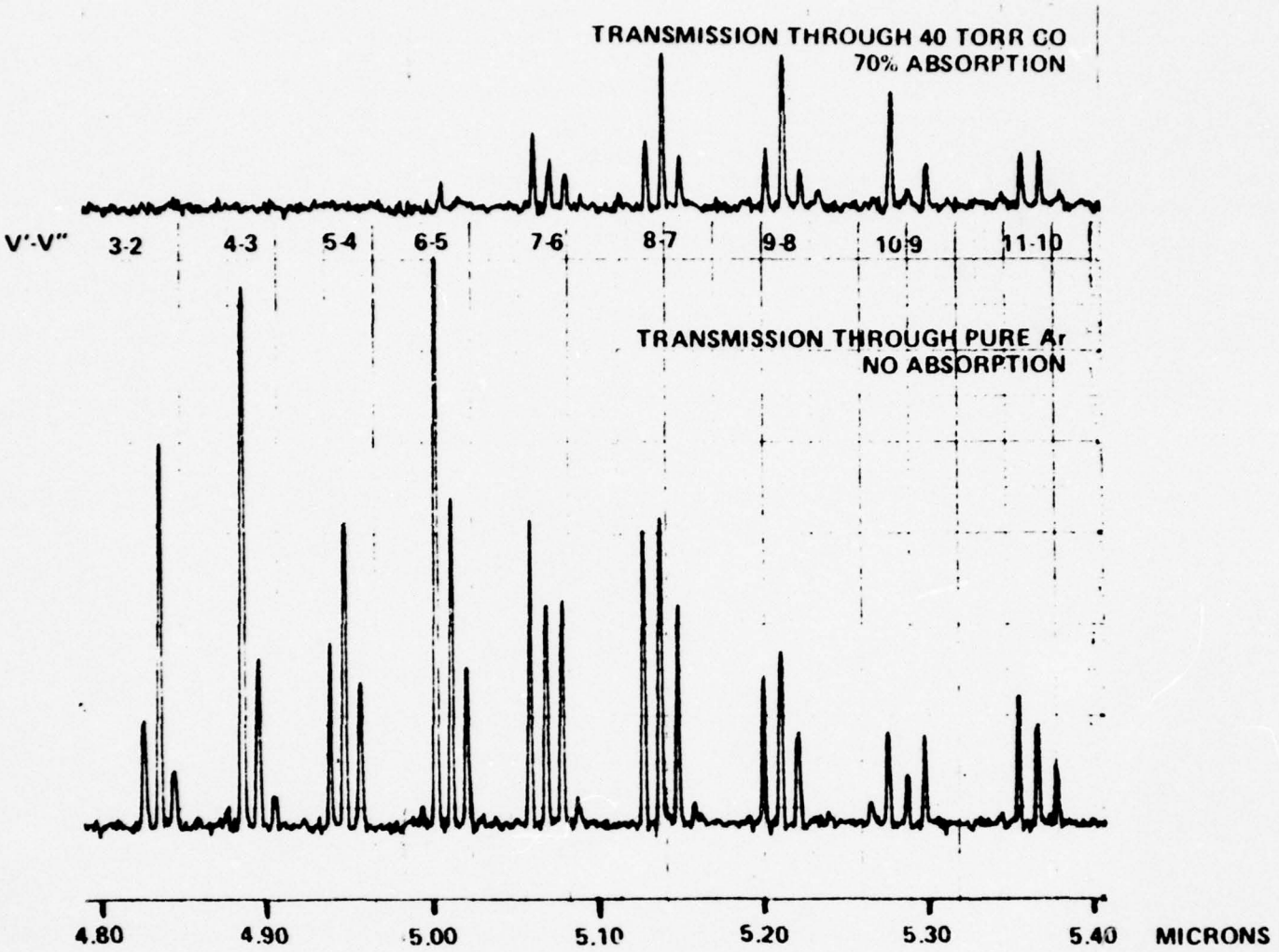

Figure 2 ABSORPTION OF PUMP LASER RADIATION SPECTRAL DEPENDENCE

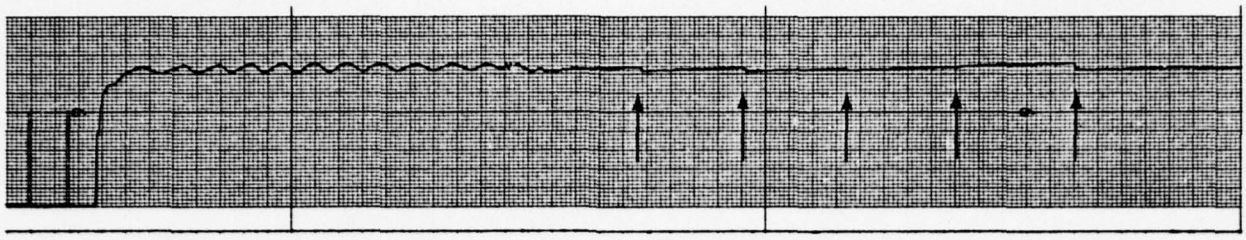

a) LASER OUTPUT, TOTAL POWER

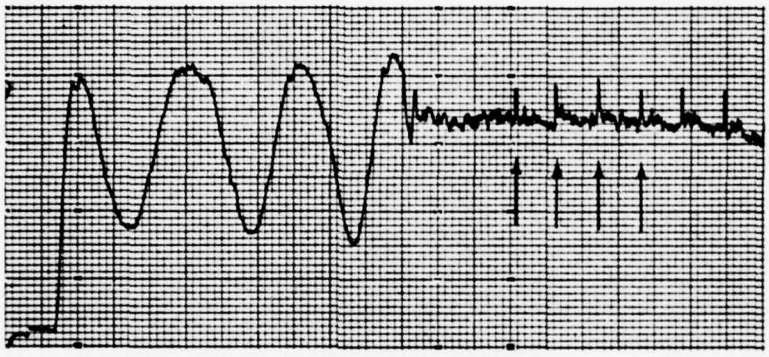

b) LASER OUTPUT, SINGLE LINE

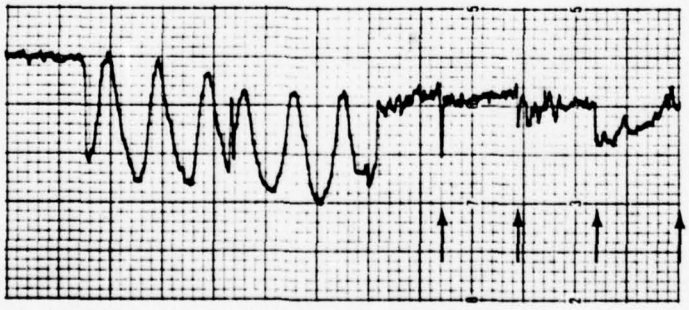

c) CELL SIDELIGHT EMISSION

Figure 3 LASER STABILIZATION; BROADBAND POWER LOCK-ON

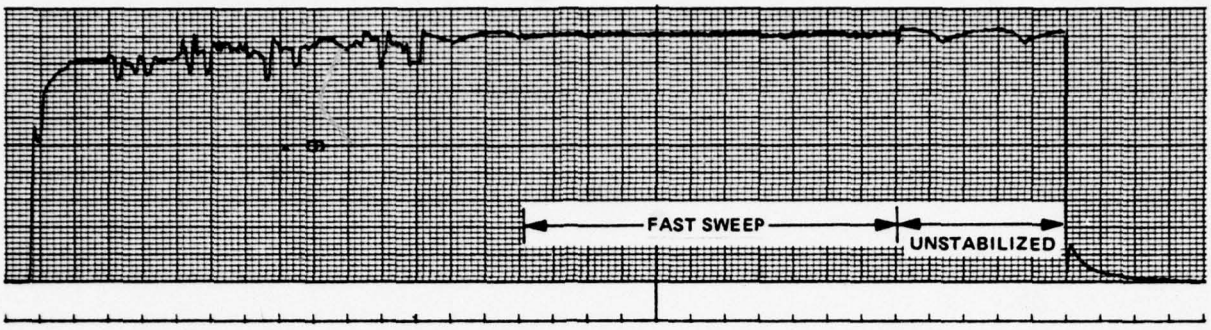

a) LASER OUTPUT, TOTAL POWER

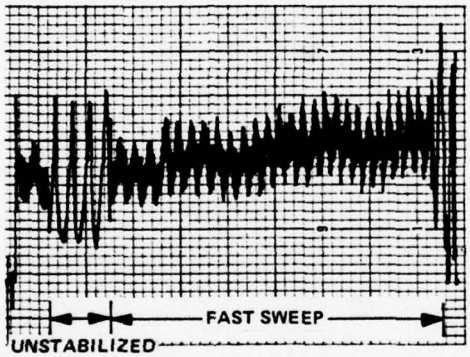

b) LASER OUTPUT, SINGLE LINE

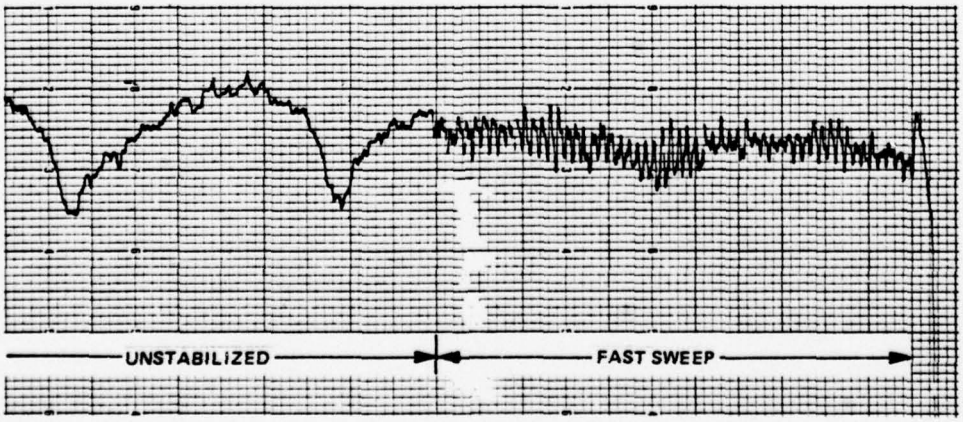

c) CELL SIDELIGHT EMISSION

Figure 4 LASER STABILIZATION; FAST SWEEP MODE

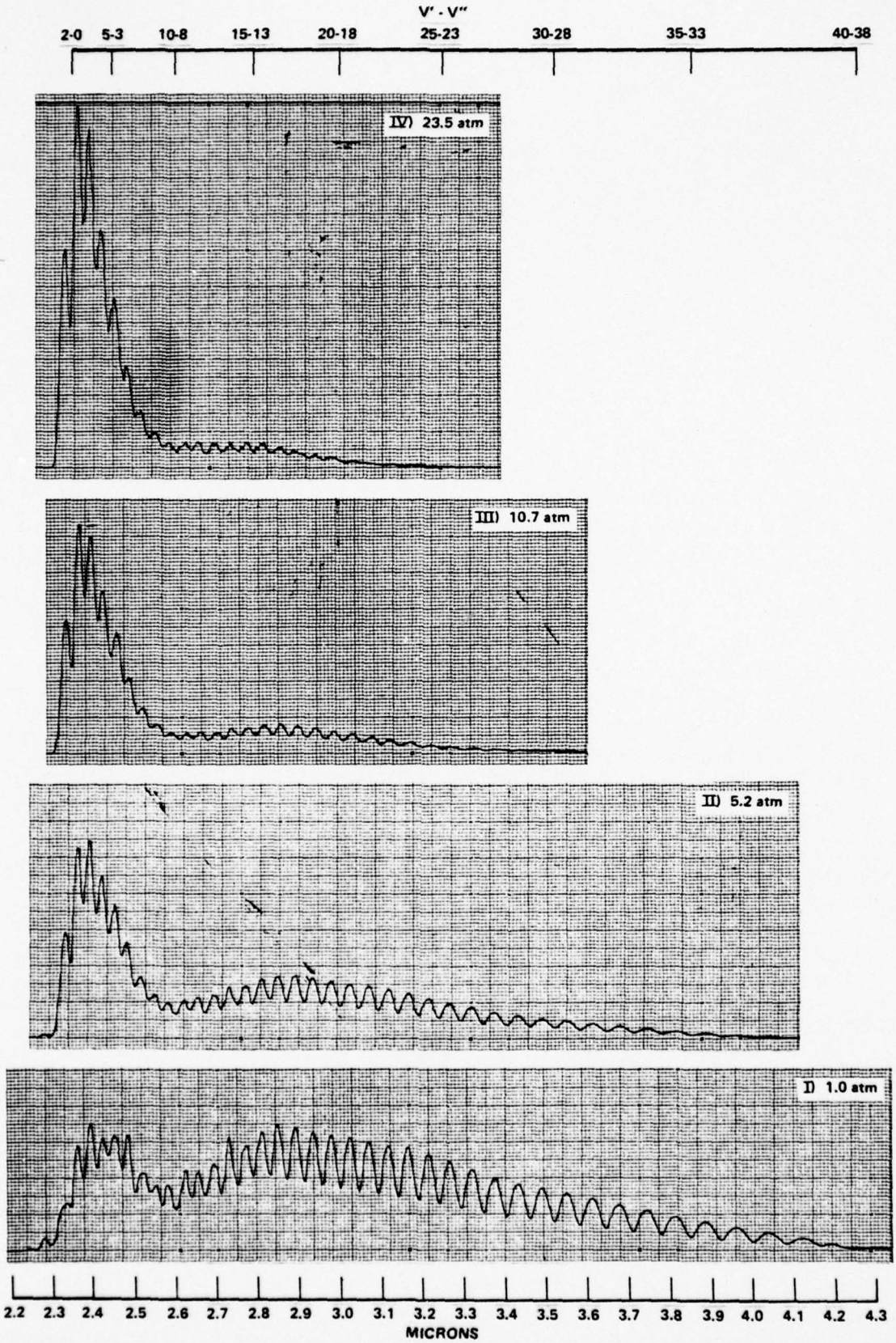

Figure 5 CO FIRST OVERTONE SPECTRA FOR SELECTED PRESSURES OF Ar DILUENT

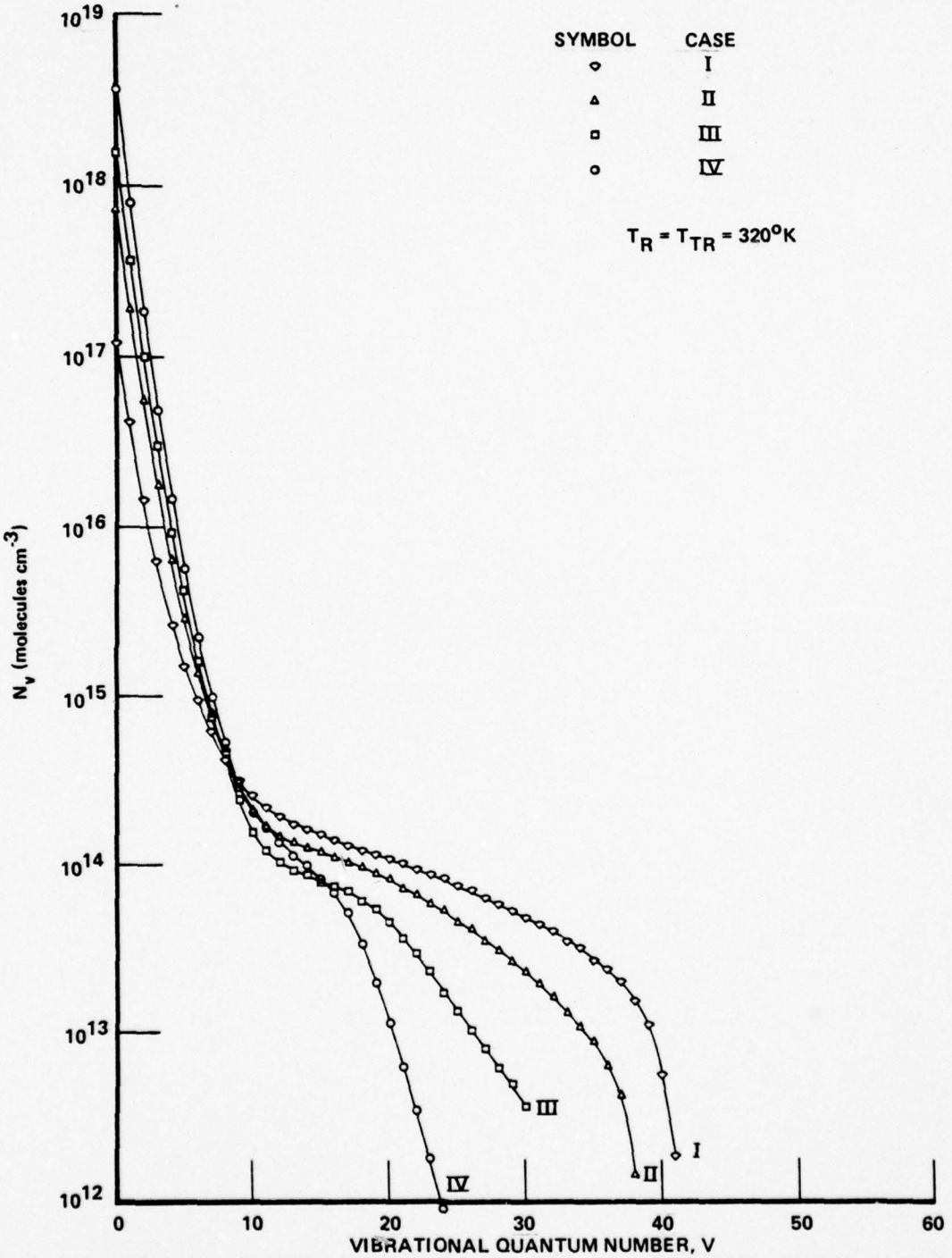

Figure 6 MEASURED CO VIBRATIONAL POPULATION DISTRIBUTIONS FOR SELECTED PRESSURES OF Ar DILUENT

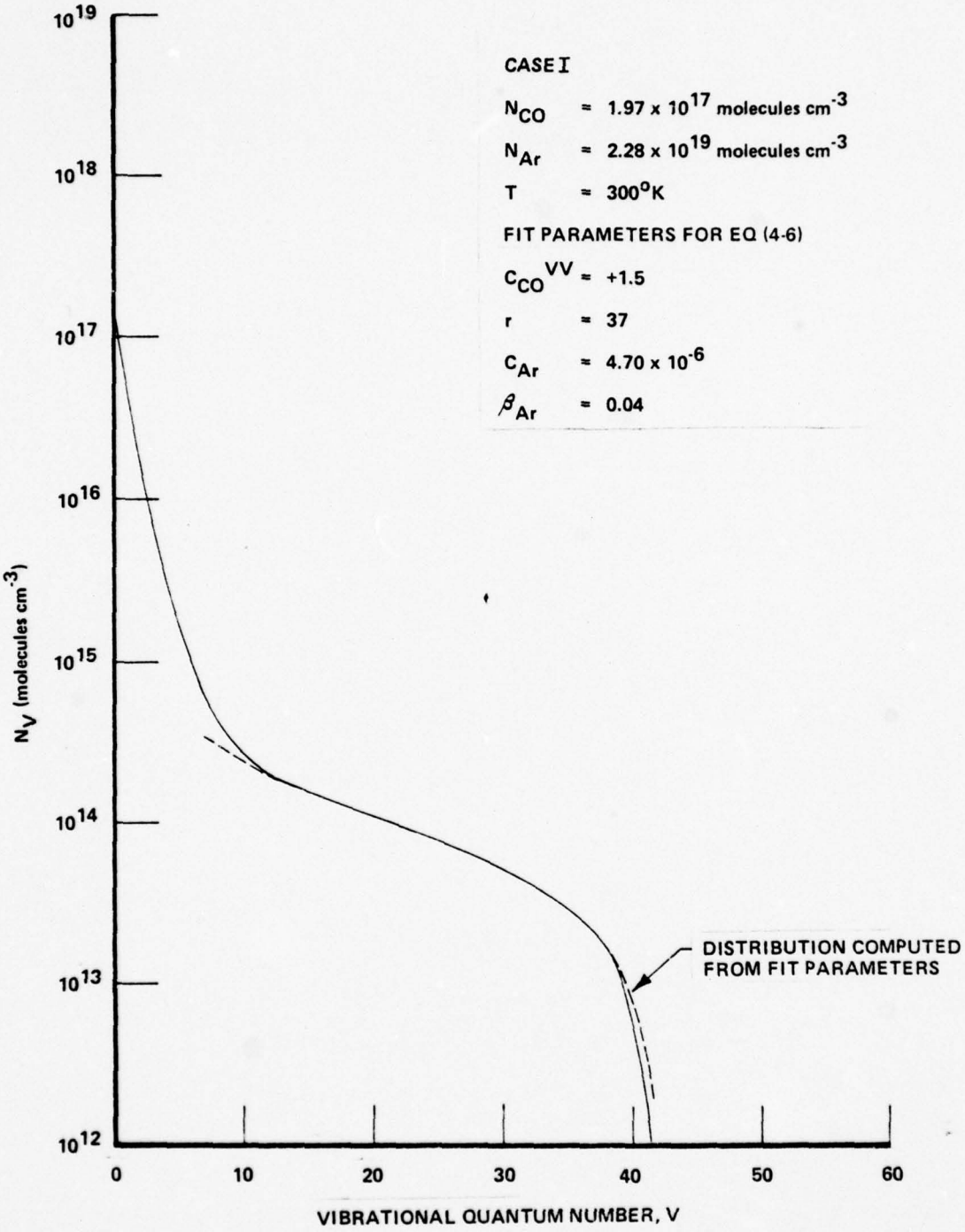

Figure 7 REDUCTION OF MEASURED DISTRIBUTION FOR CO-Ar MIXTURE, CASE I

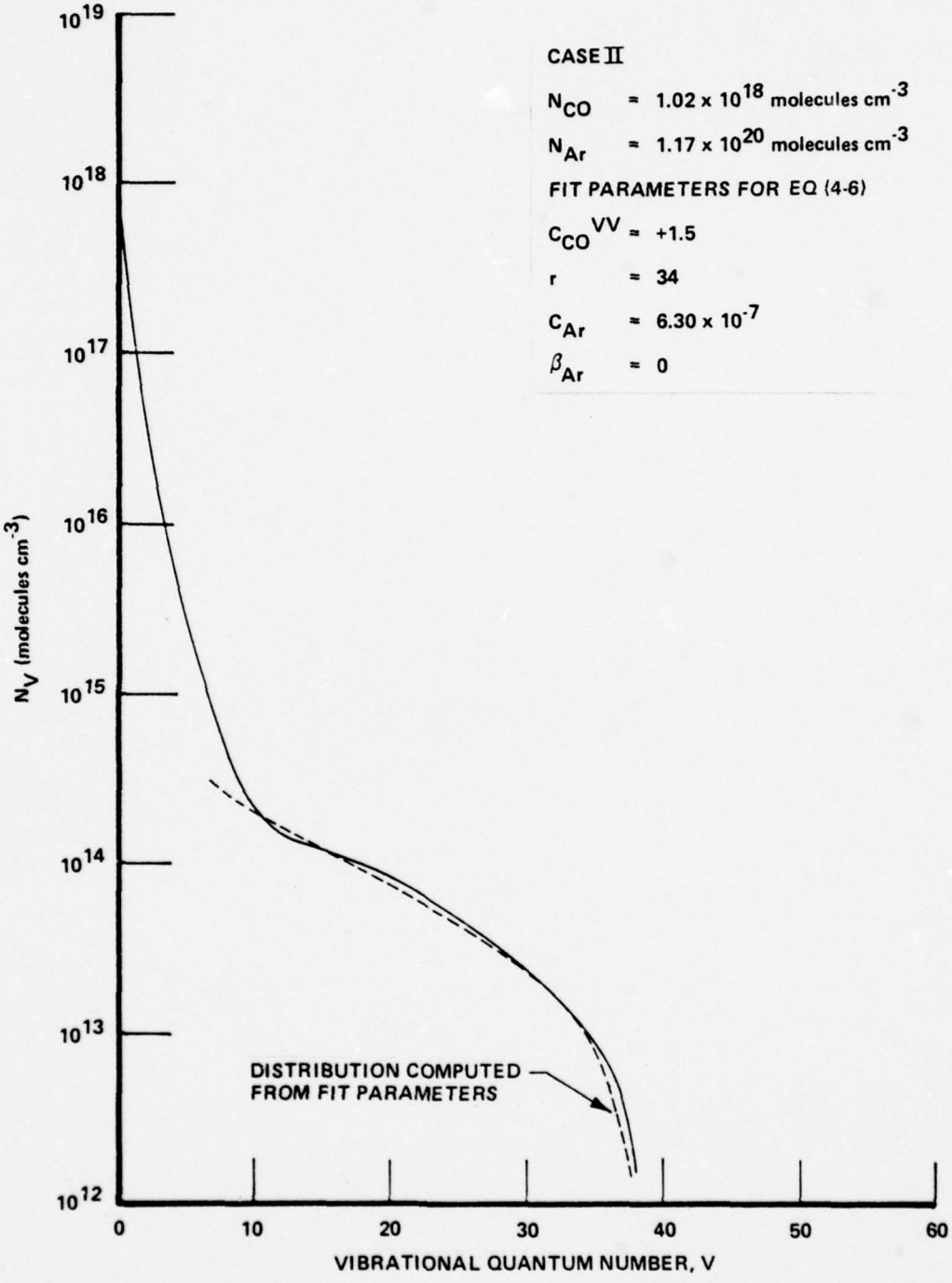

Figure 8 REDUCTION OF MEASURED DISTRIBUTION FOR CO-Ar MIXTURE, CASE II

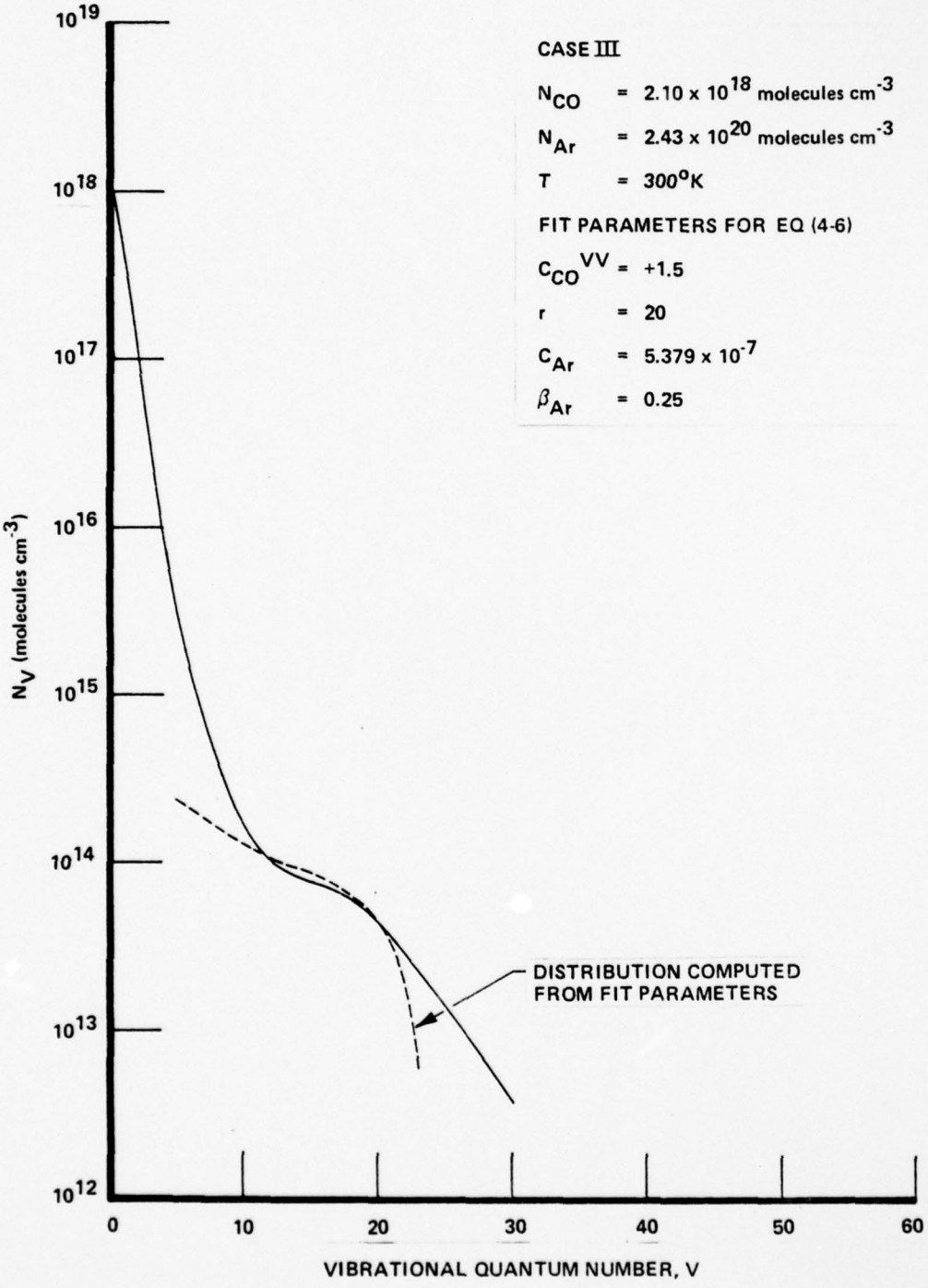

Figure 9 REDUCTION OF MEASURED DISTRIBUTION FOR CO-Ar MIXTURE, CASE III

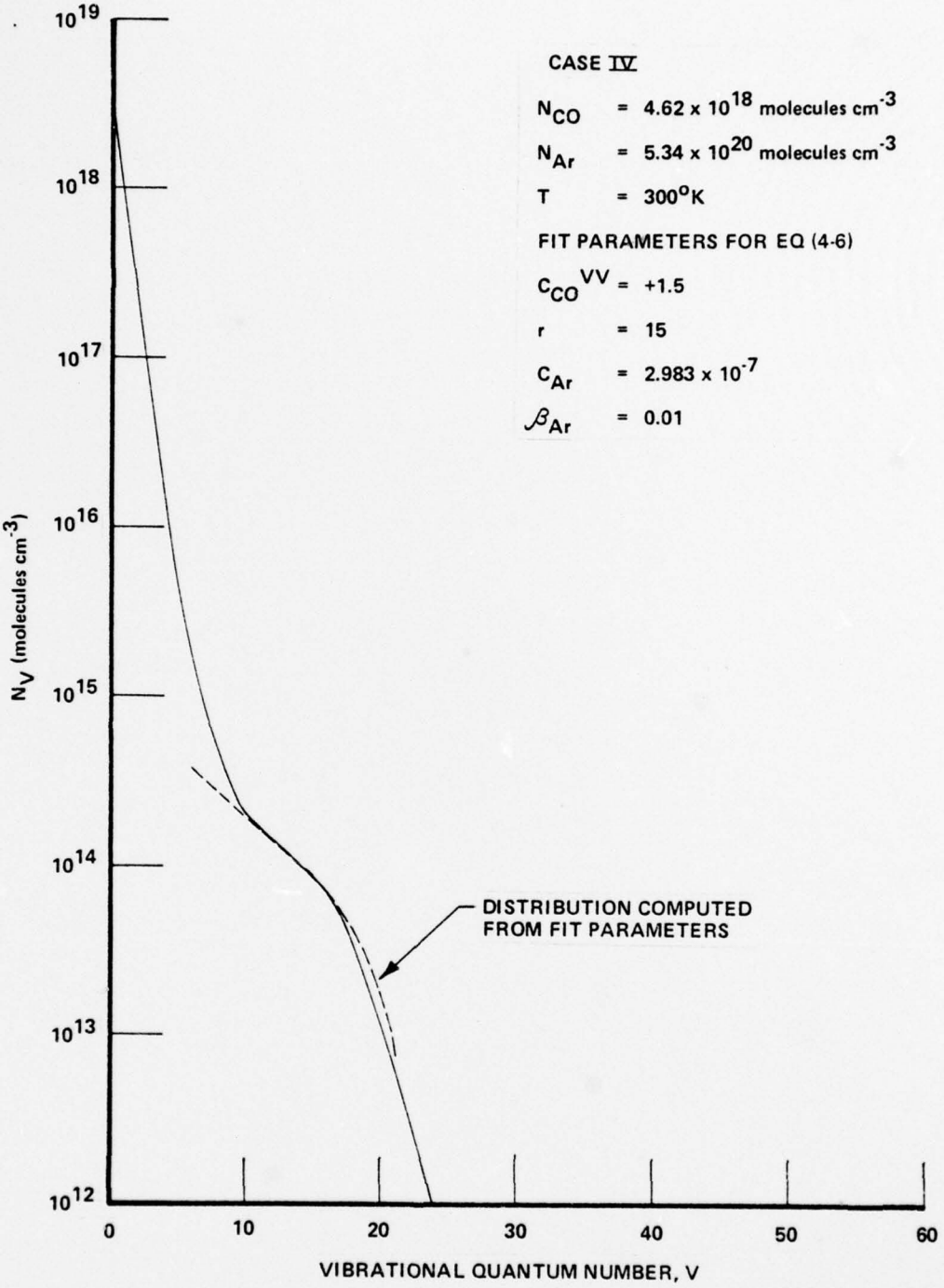

Figure 10 REDUCTION OF MEASURED DISTRIBUTION FOR CO-Ar MIXTURE, CASE IV

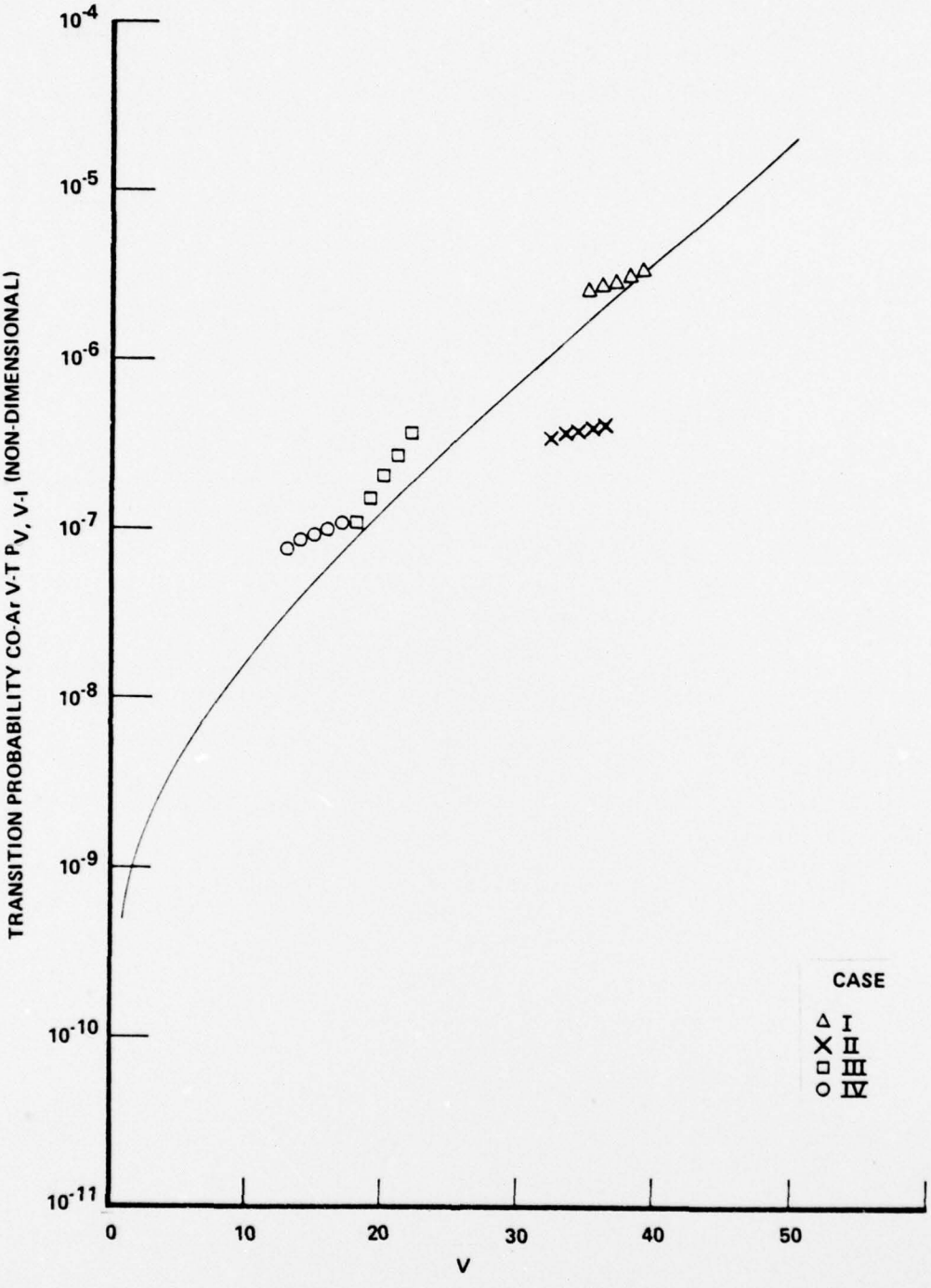

Figure 11 CO-Ar V-T TRANSITION PROBABILITY

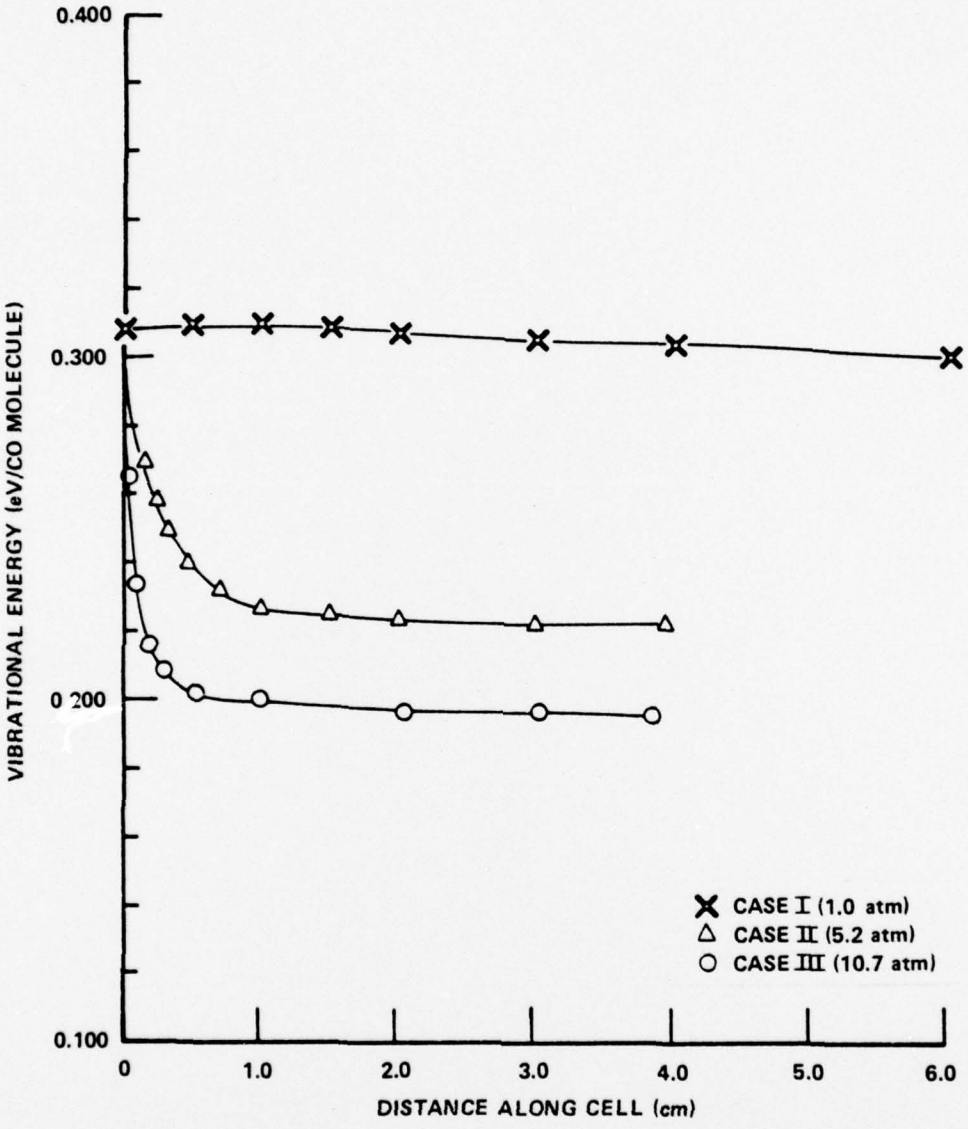

Figure 12 CALCULATED VIBRATIONAL ENERGY FOR SELECTED PRESSURES OF Ar DILUENT

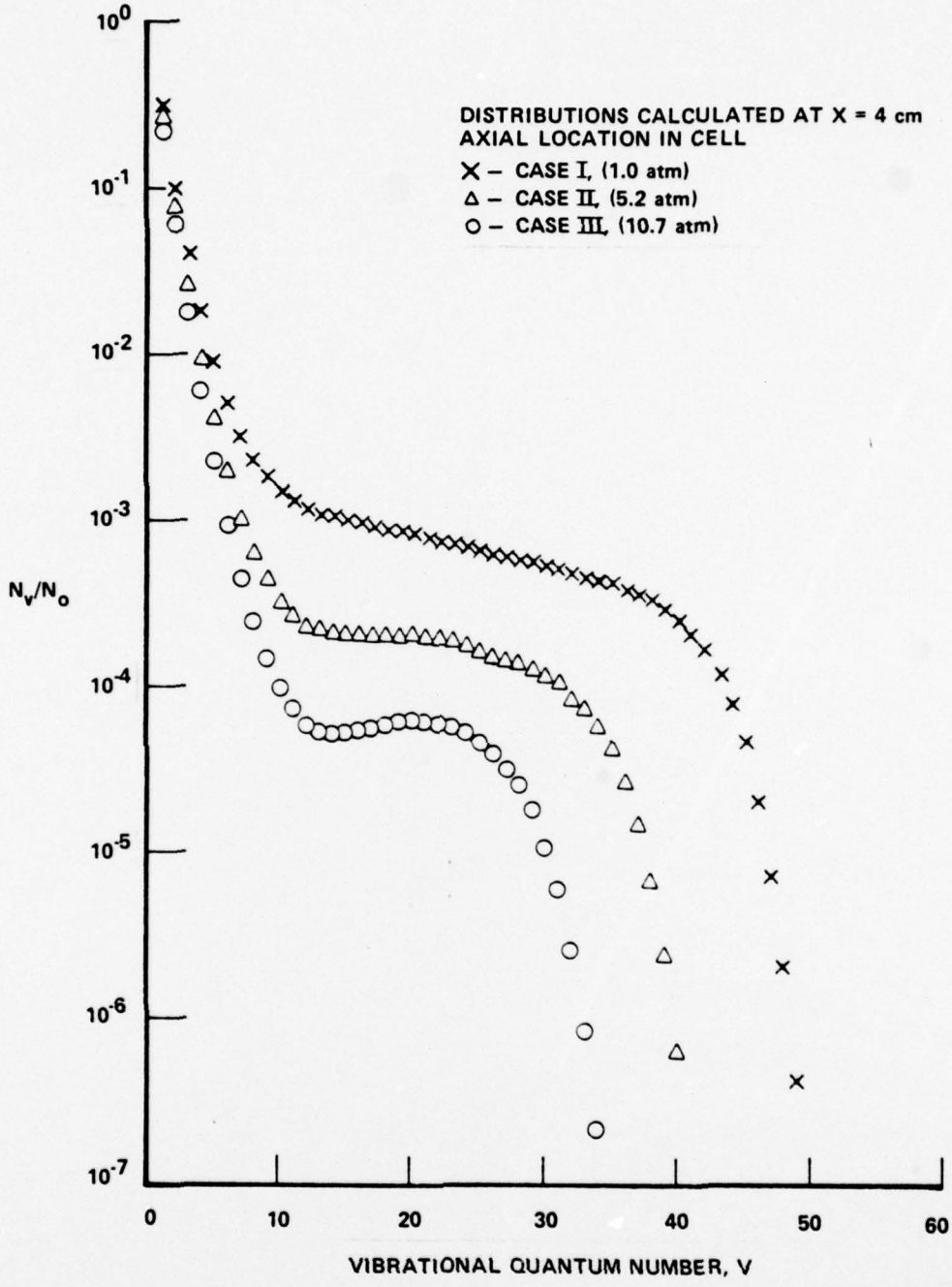

Figure 13 CALCULATED CO VIBRATIONAL POPULATION DISTRIBUTIONS FOR SELECTED PRESSURES OF Ar DILUENT

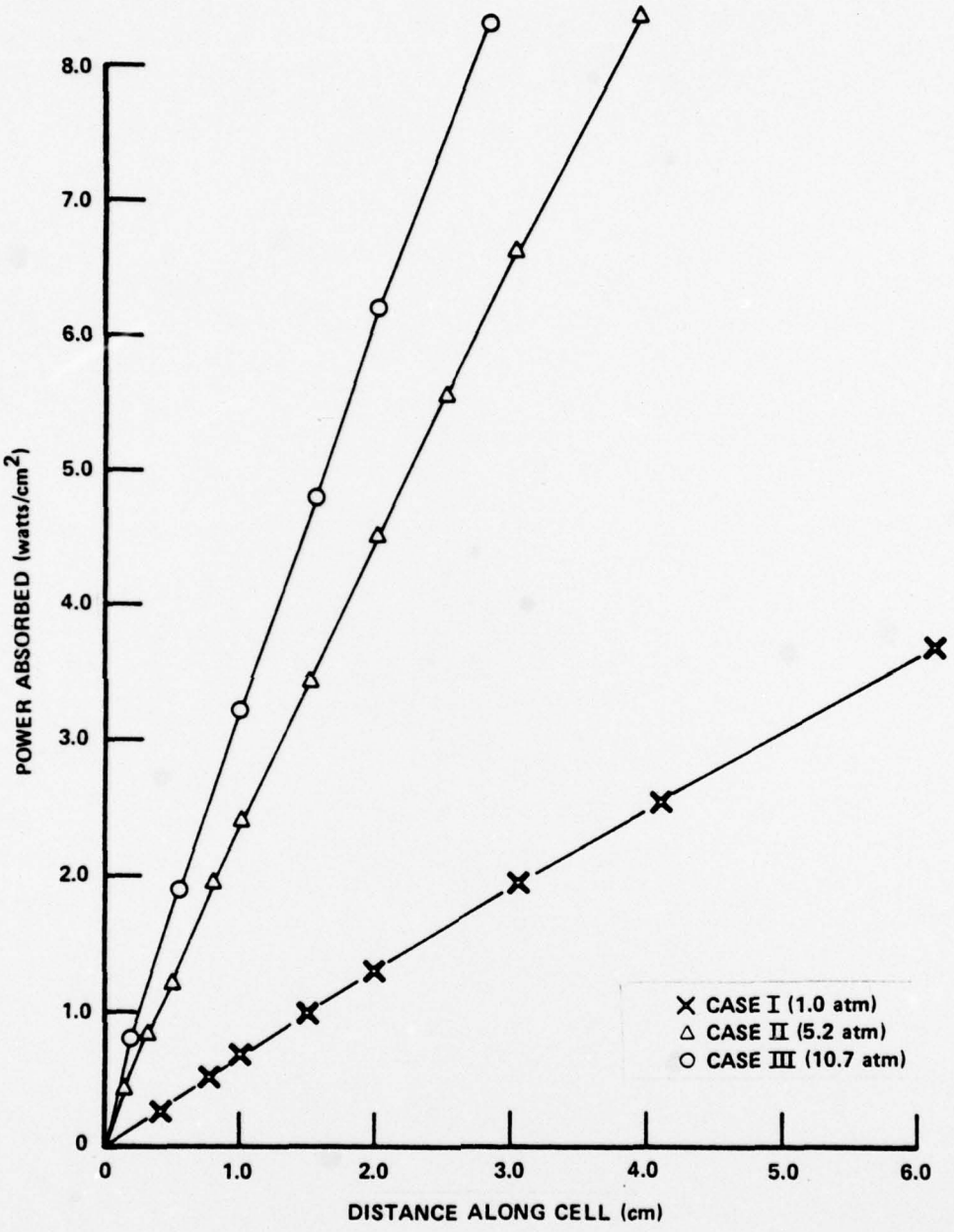

Figure 14 CALCULATED LASER PUMP POWER ABSORBED FOR SELECTED PRESSURES OF Ar DILUENT

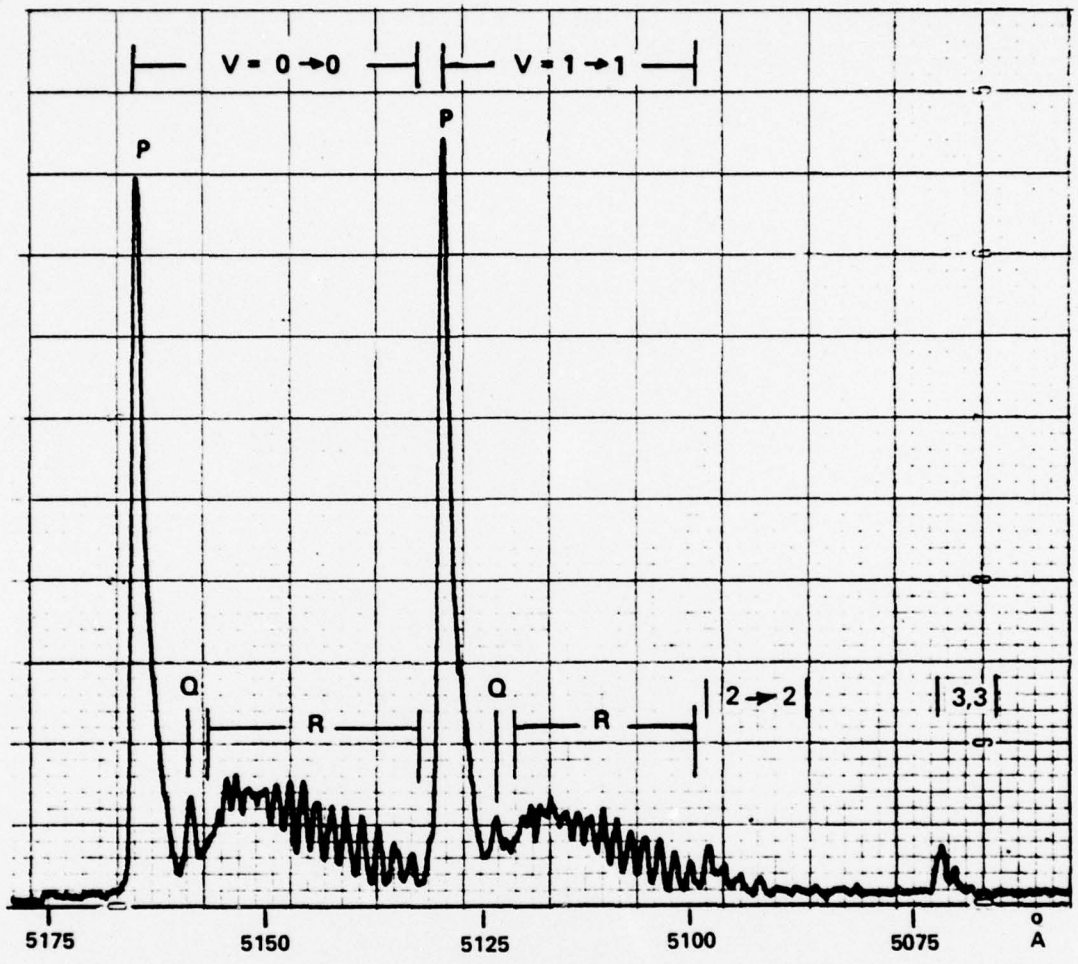

Figure 15 C_2 SWAN BANDS $(A^3\pi_g - X^3\pi_u)$
$\Delta V = 0$ SEQUENCE

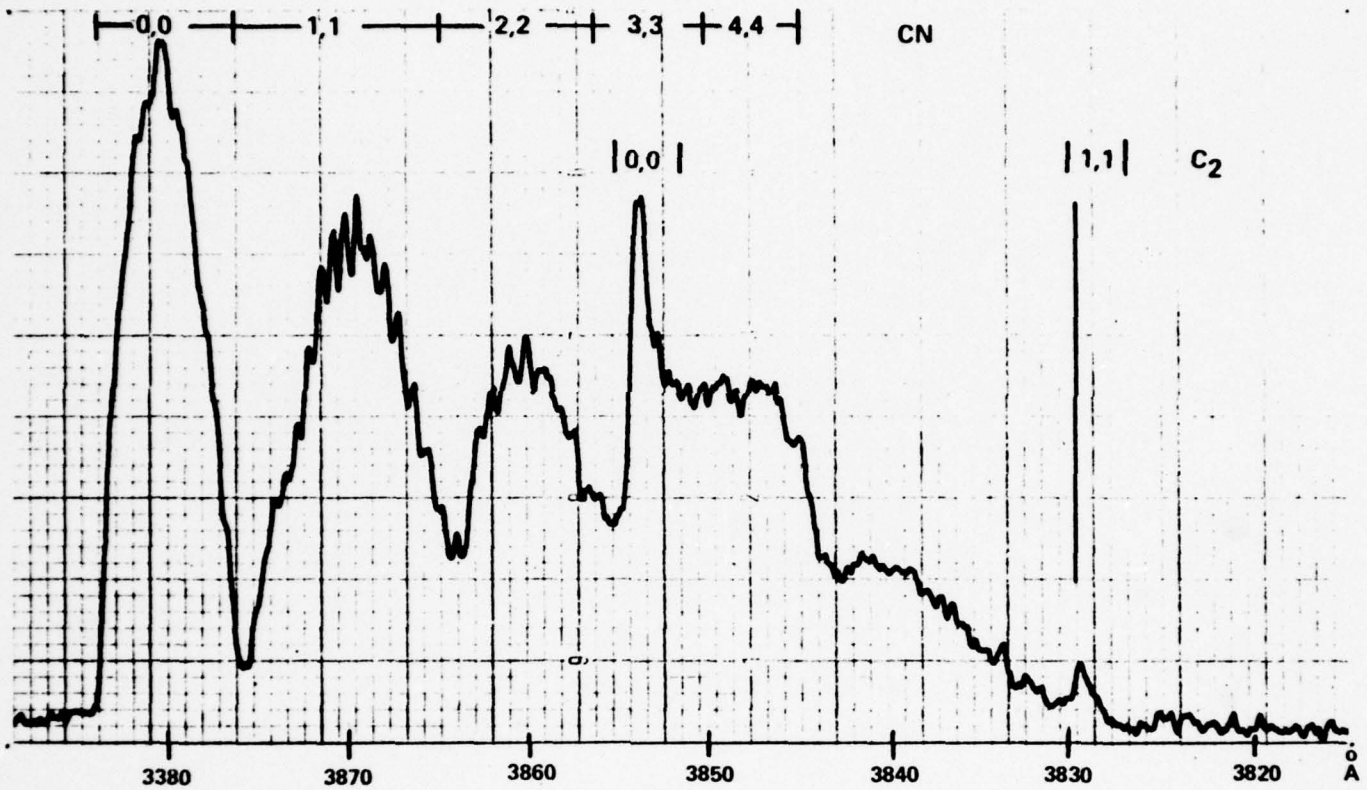

Figure 16 CN VIOLET BANDS ($B^2\Sigma^+ - X^2\Sigma^+$), $\Delta V = 0$ SEQUENCE
C_2 DES LANDRES d'AZAMBUJA BANDS ($C'\pi_g - b'\pi_g$), $\Delta V = 0$ SEQUENCE

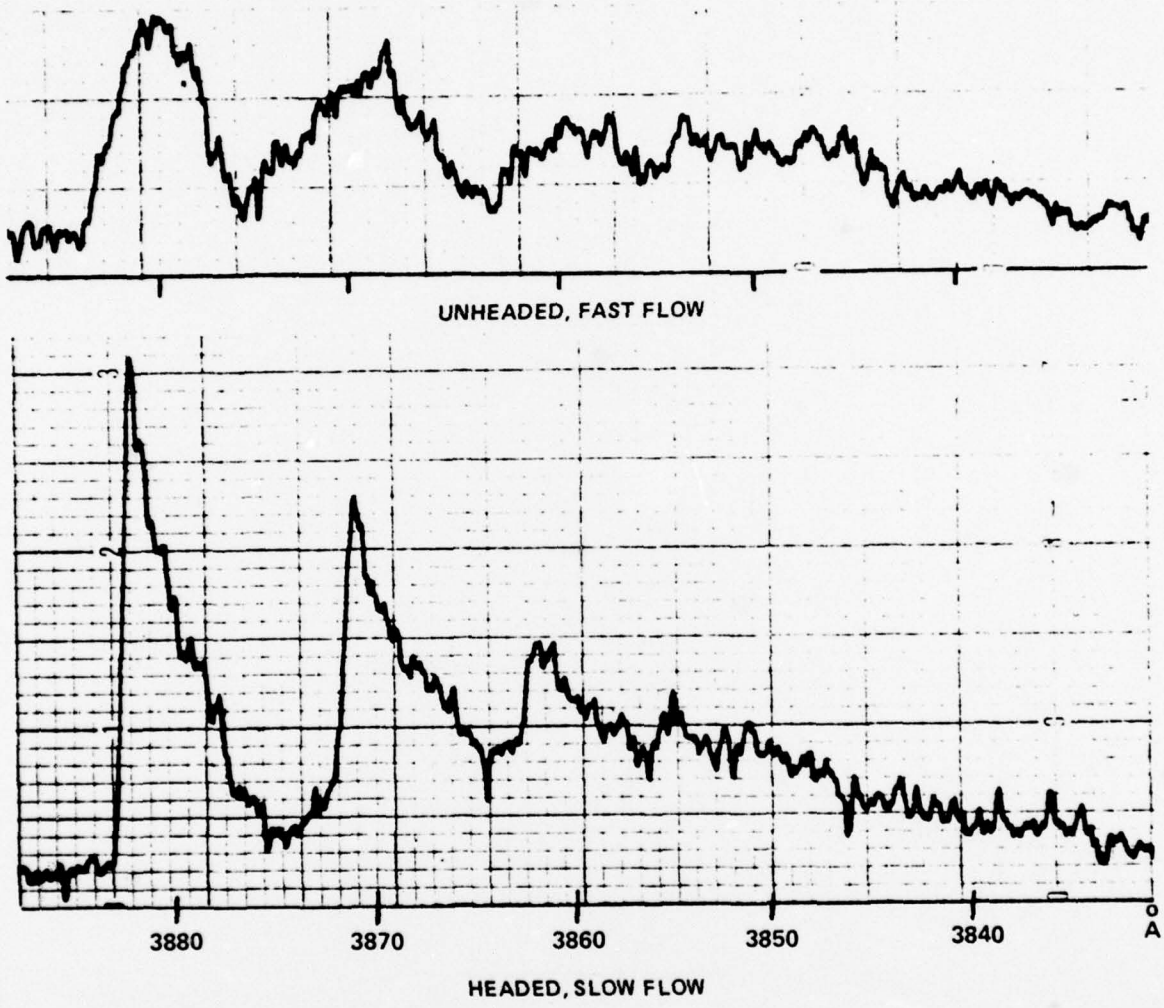

Figure 17 EFFECT OF FLOW VELOCITY ON CN VIOLET BAND HEADING

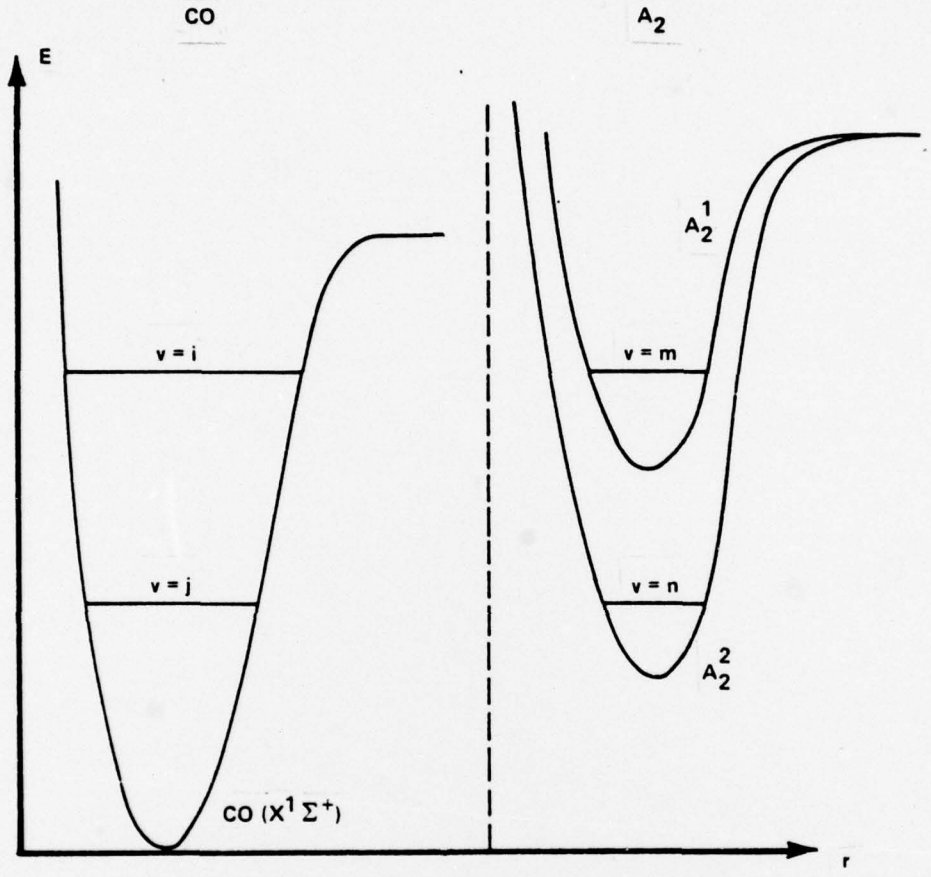

Figure 18 ENERGY LEVELS FOR MOLECULAR V-E TRANSFER PROCESS

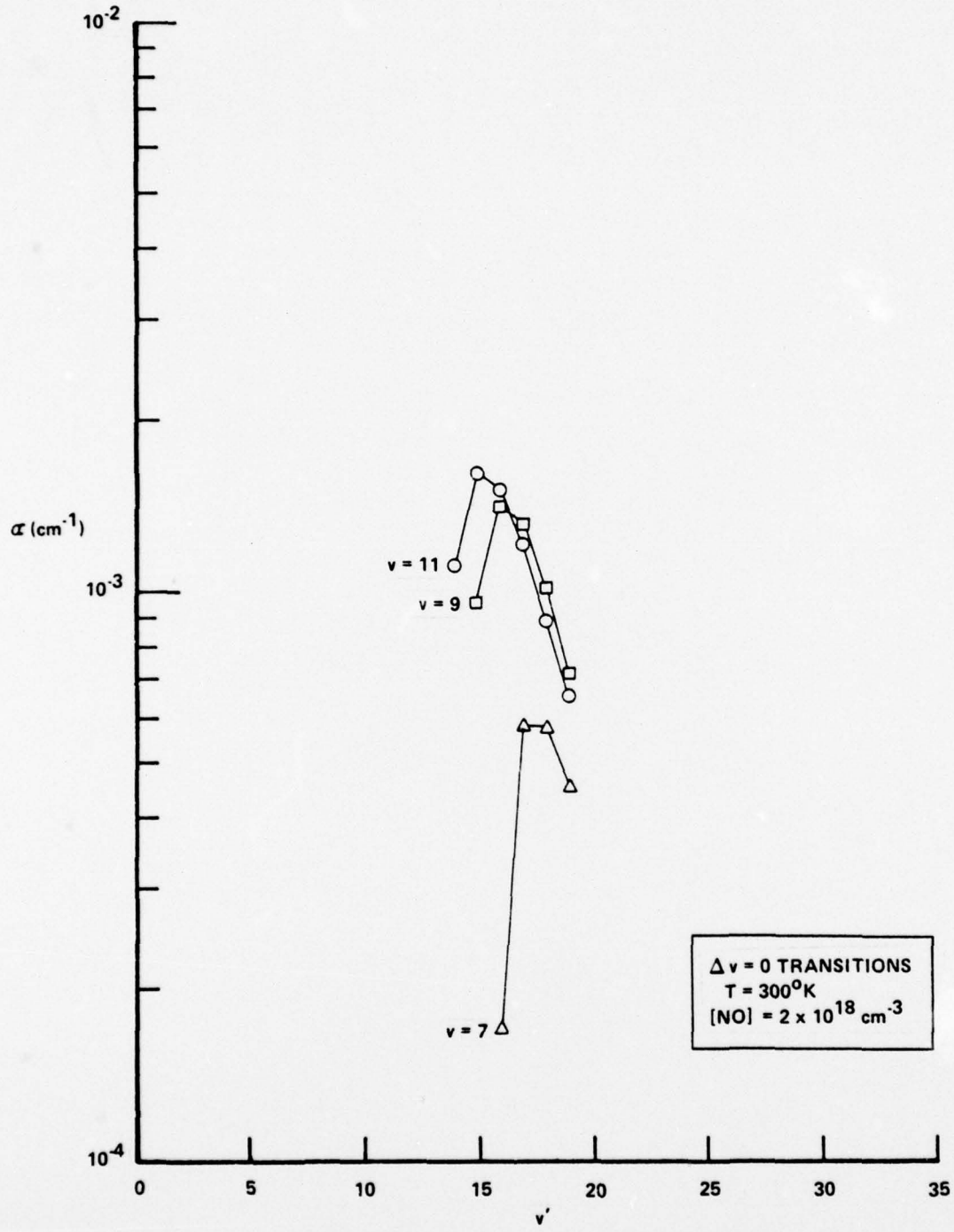

Figure 19 NO β, SMALL SIGNAL GAIN

APPENDIX A

SUMMARY OF RESEARCH PERSONNEL, PUBLICATIONS, PATENTS AND MEETING PRESENTATIONS

Participating professional personnel on this year's program were:

J. W. Rich	Project Engineer
R. C. Bergman	Research Physicist
M. W. Williams	Research Physicist
J. R. Moselle	Senior Mathematician

Publications:

1. Rich, J. W., Bergman, R. C., and Williams, M. J., "Measurement of Kinetic Rates for Carbon Monoxide Lasers", Proc. of Second International Symposium on Gas-Flow and Chemical Lasers, J. F. Wendt, Ed., Von Karman Institute for Fluid Mechanics, Rhode-St.-Genese, Belgium. In press.

2. Rich, J. W., Bergman, R. C., and Williams, M. J., "Vibration-to-Translation Energy Transfer Rates for High Quantum States of CO in Ar, He Collisions". In preparation. To be submitted to Chemical Physics or J. of Chemical Physics.

3. Rich, J. W., and Bergman, R.C., "C_2 and CN Formation by Optical Pumping of CO-N_2 Mixtures at Room Temperature". In preparation. To be submitted to Chemical Physics.

Patents:

1. Rich, J. W., Bergman, R. C., and Treanor, C. E., "Method for Initation of Chemical Reactions by Low Pressure Optical Pumping". Serial Number 833323. Application filed; notification has been received that patent will be awarded.

2. Rich, J. W., Bergman, R. C., and Treanor, C. E., "V-E Transfer Laser". Application being prepared; to be filed before 6/79.

Meeting Presentations:

1. J. W. Rich, R. C. Bergman, and J. A. Lordi, "Dissociation of Carbon Monoxide by Optically Initiated Vibration-Vibration Pumping", paper presented at 5th Conference on Chemical and Molecular Lasers, St. Louis, Mo, April 18-20, 1977.

2. J. W. Rich, R. C. Bergman, and M. J. Williams, "Measurement of Kinetic Rates for Carbon Monoxide Lasers", paper presented at 2nd International Symposium on Gas-Flow and Chemical Lasers, Von Karman Institute for Fluid Dynamics, Rhode-St.-Genese, Belgium, Sept. 11-15, 1978.

UNCLASSIFIED

SECURITY CLASSIFICATION OF THIS PAGE (When Data Entered)

REPORT DOCUMENTATION PAGE

READ INSTRUCTIONS BEFORE COMPLETING FORM

1. REPORT NUMBER: AFOSR-TR-79-0283
2. GOVT ACCESSION NO.
3. RECIPIENT'S CATALOG NUMBER

4. TITLE (and Subtitle): MEASUREMENT OF KINETIC RATES FOR CARBON MONOXIDE LASER SYSTEMS
5. TYPE OF REPORT & PERIOD COVERED: ~~Interim~~ Technical rept.
6. PERFORMING ORG. REPORT NUMBER

7. AUTHOR(s): J. W. Rich, R. C. Bergman, and M. J. Williams
8. CONTRACT OR GRANT NUMBER(s): F49620-77-C-0020

9. PERFORMING ORGANIZATION NAME AND ADDRESS:
Calspan Advanced Technology Center
P. O. Box 400
Buffalo, New York 14225

10. PROGRAM ELEMENT, PROJECT, TASK AREA & WORK UNIT NUMBERS: 2301/A1 61102F

11. CONTROLLING OFFICE NAME AND ADDRESS:
Air Force Office of Scientific Research/NP
Bldg. 410
Bolling AFB, D.C. 20332

12. REPORT DATE: November 1978
13. NUMBER OF PAGES: 65 (68 p.)

14. MONITORING AGENCY NAME & ADDRESS (if different from Controlling Office): 2301 A1

15. SECURITY CLASS. (of this report): Unclassified
15a. DECLASSIFICATION/DOWNGRADING SCHEDULE

16. DISTRIBUTION STATEMENT (of this Report)

Approved for public release; distribution unlimited.

17. DISTRIBUTION STATEMENT (of the abstract entered in Block 20, if different from Report)

CALSPAN-WG-6021-A-2

18. SUPPLEMENTARY NOTES

19. KEY WORDS (Continue on reverse side if necessary and identify by block number)

Vibrational Energy Transfer
Carbon Monoxide Lasers
Vibration-to-Electronic Energy Transfer

20. ABSTRACT (Continue on reverse side if necessary and identify by block number)

The vibration-translation (V-T) deactivation rates for high vibrational quantum levels of carbon monoxide have been measured for collisions of carbon monoxide with argon at room temperature. The rates are quantum-state-resolved and have now been measured for quantum levels from V = 10 up to V = 42. A laser optical pumping technique is used; the measurements are in an environment free of electric discharge effects.

In a related phase of the program, evidence of molecular vibration-to-electronic (V-E) energy transfer has been adduced. Preliminary analysis of this

DD FORM 1 JAN 73 1473 EDITION OF 1 NOV 65 IS OBSOLETE

UNCLASSIFIED

SECURITY CLASSIFICATION OF THIS PAGE (When Data Entered)

Cont'd on page

410 803

20.

process is given, and potential V-E transfer laser action, based on highly vibrationally excited CO, is assessed.